Elsevier Editorial System(tm) for
International Journal of Fatigue
Manuscript Draft

Manuscript Number: IJFATIGUE-D-19-00002R1

Title: Thermomechanical fatigue in 9-12Cr steels: Life prediction models and the effect of tensile dwell periods

Article Type: VSI: FDSM XII

Keywords: 9-12Cr steels; Thermo-mechanical fatigue; Dwell periods; Fatigue life prediction

Corresponding Author: Dr. Richard Allen Barrett, Ph.D

Corresponding Author's Institution: NUI Galway

First Author: Richard Allen Barrett, Ph.D

Order of Authors: Richard Allen Barrett, Ph.D; Christopher J Hyde; Padraic E O'Donoghue; Sean B Leen

Manuscript Region of Origin: Europe

Abstract: This paper is concerned with the assessment of life prediction models for thermomechanical fatigue (TMF), with specific application to P91 steel. A program of TMF tests, including dwell periods, are performed to determine the role of thermomechanical loading on fatigue life. As expected, fatigue life under conventional TMF testing (no dwells) is governed by maximum applied stress and inelastic strain-range. However, with the introduction of dwell periods, at maximum tensile stress during TMF loading, in-phase loading becomes the life-limiting case. This is attributed here to increased microstructural degradation and oxidation, associated with the dwell at peak temperature. Analysis of commonly used TMF life prediction models shows that the effect of dwell periods currently cannot be predicted for in-phase loading. Thus, it is concluded that physically-motivated approaches are required to successfully predict fatigue life under more complex (service) thermomechanical loading histories.

Response to Reviewers: Reviewer Response
The Authors thank the Reviewer for the time and effort which they obviously invested in reading, in detail, our work. This document summarises our response to the reviewer comments and highlights where changes are made. Each Reviewer comment is addressed separately. The manuscript has also been modified to reflect the comments, with the modifications highlighted in yellow. We believe that the changes made, in light of the Reviewer comments, have enhanced the quality of the submitted manuscript. Each Reviewer comment is addressed in detail below.
Reviewer #1: This is an interesting and well written paper with some important findings.
A few details must however be clarified before it can published.
Q1: Page 2, line 42: The abbreviation FCI is used but has previously not been defined.
Response: The abbreviation FCI (fatigue crack initiation) is defined on Page 2 of the revised manuscript.

Q2: Page 2, line 52: The abbreviation FI is used but has previously not been defined.
Response: The abbreviation IF (isothermal fatigue) is defined on Page 2 of the revised manuscript.

Q3: Page 3, line 5: The definition of IF is given but has already been used, see comment 2.
Response: The definition of IF has been moved forward in the revised paper as per comment 2.

Q4: Page 4, section 2.2: The failure criteria for fatigue life should preferably be given in this method section, not in the results section.
Response: The failure criteria for fatigue life is now moved to the experimental methodology section (Section 2.2) on page 4 the revised manuscript.

Q5: Page 5, section 2.2: The dwell time for the TMF-OP tests is applied at Tmin. This is perhaps not the most common TMF-OP dwell cycle. Often the dwell is applied at Tmax in both IP and OP test and thus at compressive stress for OP tests. However, the cycle the authors have used might very well be relevant for a specific application. But I would like to see that this is clearly pointed out in section 2.2 and perhaps also motivated.
Response: The authors agree that the proposed cycle is not the conventional TMF-OP cycle with a dwell at maximum temperature (maximum compressive stress). However, this cycle, with a dwell at Tmin, is selected as it is representative of part-load operation in power plant, where the temperature undergoes a dwell period at a lower temperature similar to the Tmin values considered here. Under such conditions, the operating pressure can increase, hence, generating a CTMF-OP cycle similar to that presented here. The following text has been added on page 4 of the revised manuscript to highlight this point:
"Similar to the IF test program, the CTMF test also has a dwell period at maximum tensile strain, corresponding to a dwell at maximum temperature, Tmax, for IP conditions and at minimum temperature, Tmin, for OP conditions. Although a dwell period at Tmax is a commonly used OP cycle, the proposed OP cycle (with a dwell period at Tmin) is designed to represent part-load operation of power plant. Dwell periods under such conditions occur at a reduced operating temperature similar in magnitude to the Tmin value of 673 K tested here."

Q6: Page 5, line one: The authors state that the relaxation during dwell for the CTMF tests is consistent with the CF tests. But from Figure 5 I would say that there is a slight difference for the CTMF-IP test and the CF-873K test.
Response: The authors agree with the Reviewer that there are differences between the CTMF-IP test and the CF-873 K test. This difference is attributed here to the strain-rate effect. To demonstrate this effect, additional data at an alternate nominal applied strain-rate is included for CTMF-IP and CTMF-OP loading conditions. For the CTMF-OP conditions, where the dwell temperature is 673 K, no significant effect is observed, consistent with IF test data at the different strain-rates considered

here. However, for CTMF-IP conditions, where the dwell temperature is 873 K, a clear effect with strain-rate is observed, consistent with the observed effect under IF test conditions at 873 K. The CF-873 K test was conducted at a strain-rate of 1×10-3 s-1, whereas the CTMF tests are conducted at lower strain-rates of 3.3×10-4 s-1and 2.5×10-4 s-1. The text on pages 5 and 6 of the revised manuscript has been modified to clarify this as follows:
"The measured stress relaxation during the dwell period of the CTMF tests is presented in Figure 7 for both OP and IP loading conditions. A comparison with isothermal CF experimental data at the dwell temperatures of 673 K and 873 K, respectively, is also presented. To enable a direct comparison of relaxation behaviour across a range of strain-rates, this data is normalised by the stress at the start of the hold period (σ0). During this isothermal dwell period in the CTMF cycle at the same applied mechanical strain, the observed relaxation of stress in each case is similar to that of the isothermal CF tests at 673 K for the OP case, as presented in Figure 7a. However, there exists a significant difference in relaxation behaviour for dwells at 873 K (Figure 7b). For the strain-rates considered here, no significant strain-rate effect is observed in P91 steel at temperatures below 773 K [7]. However, a significant strain-rate effect is observed in P91 steel under IF at 873 K, as presented in Figure 8a. Thus, it is concluded here that the observed trend in Figure 7b is primarily due to the strain-rate effect under higher dwell temperatures."

Q7: Page 5, line 6-8: In this section the strain rate effect is discussed for TMF-IP, Figure 6b, but the sentence ends with a statement that dwell occur at 873K. Why did you chose to study the strain rate effect for tests that also included a dwell. Also the caption for Figure 6b indicate that this is the CTMF tests and the labels indicate two different strain rates. However this is not consistent with the test conditions in Table 1, which indicates that the CTMF test were done with just one strain rate?
Response: The effect of nominal applied strain-rate in a dwell test is included to investigate if the applied strain-rate has an effect on the relaxation behaviour of P91 steel. This effect is now presented in an updated Figure 5 (see comment Q6). These results will also be exploited in future modelling work on the evolution of the thermal stress component under different loading cycles.
The test conditions in Table 1 have also been updated to include all strain-rates at which CTMF tests were performed.

Q8: Page 5, line 37-40: Move this to the method section, see comment (4)
Response: The failure criteria for fatigue life is now moved to the experimental methodology section (Section 2.2) on page 4 of the revised manuscript.

Q9: Page 5, line 43 and Figure 10: All IF tests are plotted together with one colour, independent of test temperature. Is there not any systematic difference between the different test temperatures? If so I think this is an important finding that you could highlight more clearly.
Response: The IF tests of Figure 10 (Figure 11b in the revised manuscript) are now plotted with different symbols to denote the three different test temperatures. However, when plotting inelastic strain-range versus Nf, the IF test data essentially collapses to a linear fit

on a log-log plot (power law relationship). This temperature-independent power law relationship also simplifies the parameter identification process for the failure models under TMF.
Furthermore, although there is not a clear temperature effect for inelastic strain-range versus Nf, a clear temperature-dependence exists when applied mechanical strain-range versus Nf is plotted. This temperature-dependence is presented in Figure 11a of the revised manuscript.
The following text has also been included on pages 6 and 7 of the revised manuscript to clarify this finding:
"It should also be noted that there is a significant temperature-dependence for the number of cycles to failure as a function of the applied mechanical strain-range for IF conditions (Figure 11a). However, this temperature-dependence is not as evident when considering inelastic strain-range versus Nf, where the IF test data essentially collapses to a power law relationship as shown in Figure 11b."

Q10: Page 5, line 54: The definition for the abbreviation FCI is given but has already been used before, see comment (1)
Response: The definition of FCI has been removed from this section in the revised manuscript.

Q11: Page 6, line 2: The authors state that there is a significant different relationship with inelastic strain-range for the symmetric and asymmetric TMF-IP tests. But judging from figure 10 I don't think the authors have enough data to really say that this is a significant difference.
Response: The deviation from a power law relationship at the lower applied strain-ranges is possibly due to the transition from low-cycle fatigue to high-cycle fatigue. The text on page 7 of the revised manuscript has been modified to provide this explanation for the deviation from power law behaviour and to highlight that further testing is required to confirm this is the transition region:
"This may represent the transition from low-cycle fatigue to high-cycle fatigue for P91 steel. Thus, further testing at these lower applied strain-ranges under IF and TMF (both symmetric and asymmetric) test conditions is required to define whether this is the transition region for low-cycle fatigue to high-cycle fatigue; this will also provide essential data for plant designers and fatigue life prediction at these potentially crucial strain-ranges for conventional power plant applications."

Q12: Page 6, lines 4-19: Here it is very confusing again regarding the variation in strain rate for the CTMF tests. Figure 12 gives data for two different strain rates, but no information about the strain range is given is it the same?
Response: The applied strain-range (±0.5%) is now included in the caption of Figure 12 (Figure 13 in the revised manuscript).

Q13: What is the difference between the TMF tests in Figure 17b and Figure 18a. The cycles to failure seems to be different but the description indicate that it is the same kind of tests so why are all data not plotted at the same time. Also all data from the tests are not given in the paper, basic stuff like strain ranges vs cycle to failure is

missing. Unfortunately, this creates some suspicious feelings to an otherwise very good paper.
Response: The plot of applied mechanical strain-range vs cycles to failure is now included in Figure 11a of the revised manuscript. Figure 17b presents the application of the Zamrik model to the IF and symmetric TMF tests only. Figure 18a is application of the Zamrik model to the asymmetric TMF tests only. This data, and TMF loading with dwells, were split into individual plots to investigate the capability of the Zamrik model to predict fatigue life under (i) IF and symmetric (conventional) TMF, (ii) asymmetric TMF and (iii) CF and CTMF conditions. The text on page 8 of the revised manuscript now makes this distinction.

Reviewer #2: The work reported in the manuscript is a useful addition to the published literature and will assist researchers in understanding the TMF response of an important alloy. Several minor comments should be addressed however prior to publication.
Q1: In the abstract, "state of the art TMF life prediction models" are referenced, however the manuscript seems to deal with fairly standard life correlation parameters (Coffin-Manson, for example). Could the authors please clarify what is state of the art about the application?
Response: The state-of-the-art aspect was focused on current design standards for fatigue analysis of power plant components (e.g. ASME boiler codes). However, the text on page 1 of the revised manuscript has been updated to clarify this statement and now defines the models as "commonly used TMF life prediction models".

Q2: In the final paragraph of the introduction, it is stated that the effect of phase angle has not been investigated in TMF lifing. It should be noted here, to avoid all ambiguity, that this observation is made in reference to P91. Phase angle effects in TMF have certainly been investigated for other alloys.
Response: The text on page 3 of the revised manuscript has been updated to clarify that the effect of phase angle has not been investigated for TMF with dwells for 9-12Cr steels.

Q3: In the experimental testing section, please explain why loading ratios of -0.4 and -0.2 were used? Is this based on predicted power plant load waveforms?
Response: The loading ratios of -0.4 and -0.2 are based on component level modelling predictions for P91 header components [Farragher et al., 2013]. Farragher and co-workers presented predicted thermo-mechanical stress-strain response at a number of locations in a header unit under measured plant start-up thermal histories. The loading ratios of -0.4 and -0.2 selected in the present work represent the approximate upper and lower bounds of the predicted hoop and axial stress-strain responses at specific locations in a header unit. The text in the revised manuscript has been updated on page 4 to clarify the selection of loading ratio: "Asymmetric TMF tests, where the maximum tensile strain is significantly higher than the maximum compressive strain, were also performed with Rε-ratios based on predicted strain in the hoop and axial directions for finite element modelling of a header unit under representative (measured) cyclic operation [3]. Thus, the asymmetric TMF tests were performed under IP and OP conditions, with Rε-ratios of -0.4 and -0.25, representing the upper and lower bounds of the finite element predicted Rε-ratios."

Q4: The final few sentences of paragraph 1 in section 3.1 are a little unclear and should be revised. I believe that the authors are trying to suggest that strain rate sensitivity is not observed as the specimens in question only spend a limited amount of time above 773K. The difference between loading rates applied in fig 4 are very small compared to the differences suggested between in service components and laboratory tests, so a limited sensitivity here is not too surprising. From the reviewers own experience, P91 exhibits strain rate dependency even at 673K.
Response: The authors agree that strain-rate dependency occurs at temperatures much lower than 873 K. However, for the strain-rates considered here, a minimal strain-rate effect is observed over the relatively narrow range of intermediate to high temperatures and strain-rates considered here. The text in Section 3.1. on page 5 of the revised manuscript has be updated to reflect this.

Q5: Please indicate how the inelastic strain range is calculated for determining p (see the last paragraph of section 3.1). The inelastic strain range will of course evolve as the material hardens and, for P91, a stabilized state is never actually achieved (this is observed in fig 6 (a) and fig 7 (b)). The expression for p suggests that an average value for the inelastic strain range is used but it is unclear how this is determined. A similar question can be posed in relation to the maximum stress terms used in equations 2, 3, and 4.
Response: The inelastic strain-range, $\Delta\varepsilon_{in}$, is taken as the difference between the maximum and minimum strain at zero stress in the measured stress-strain hysteresis loop. This inelastic strain range is a function of cycles. The accumulated inelastic strain is twice the summation of inelastic strain range over a number of cycles. This expression has also been clarified in the revised manuscript. The following text has been added on page 6 of the revised manuscript to clarify the definition of p: "Figure 9b presents the accumulated inelastic strain, $p=2\sum_{i=1}^{N_f}\Delta\varepsilon_{in,i}$, where Nf is the number of cycles to failure and $\Delta\varepsilon_{in,i}$ is inelastic strain range for cycle i, as defined in Figure 10 for CTMF-IP and CTMF-OP loading and comparisons with the corresponding CF data at 673 K and 873 K."
In Equations (2) to Equation (4), the maximum stress, σ_{max}, and inelastic strain range, $\Delta\varepsilon_{in}$, for model parameter identification (only) are taken to be the experimental values at half-life, as documented in Section 3.4 of the revised manuscript.

Q6: In the conclusions, the authors recommend that inelastic strain energy based models should be used with caution as they break down when significant dwell periods are applied. The experimental work only considers 2 minute hold periods however. The header components referenced at the start of the paper may well operate for a few hours at constant load (a dwell condition). Can the authors please reconcile this?
Response: Previous CF testing by this group on a different 9Cr alloy with a 1 hr dwell period [4], highlights that the stress relaxes asymptotically in 9-12Cr steels, rapidly decaying to the saturated value over a short period of time (on the order of a few minutes). Thus, the dwell tests conducted in this study can qualitatively capture the evolution of the thermal stress. However, an ongoing test program for another 9-12Cr alloy will specifically look at the effect of dwell time

(with dwells ranging from 2 minutes to 2 hrs) on microstructural degradation and fatigue life.
The following text, on page 10 of the revised manuscript, has been included to reconcile the 2 minute dwell with typical dwell periods in realistic plant components:
"Although conventional power plant components tend to operate with dwell periods on the order of hours, a significant proportion of the thermal stress component relaxes during the initial (rapid) stage of a hold period. For 9-12Cr steels, this initial stage of stress relaxation is on the order of minutes with the stress rapidly decaying to a saturated value [4]. Hence, the 120 s dwell period considered here can qualitatively capture the relaxation behaviour of P91 steel. However, future work will also investigate the effect of dwell time on CF and CTMF performance in 9-12Cr steels to determine the role of microstructural degradation during dwell periods on fatigue life."
Furthermore, the conclusions on page 11 of the revised manuscript have also been updated to state more specifically that the inelastic strain energy-based models break down for "higher temperature dwell periods".

Dear Sir/Madam,

Thermomechanical fatigue in 9-12Cr steels: Life prediction models and the effect of tensile dwell periods

Richard A. Barrett, Christopher J. Hyde, Padraic E. O'Donoghue, Sean B. Leen.

Please find enclosed the above-titled paper which we wish to submit for publication in your journal.

The referees that we recommend are:

[1] Dr. Jürgen Olbricht
Federal Institute for Materials Research and Testing, Berlin, Germany
juergen.olbricht@bam.de

[2] Dr. A. Nagesha
Metallurgy and Materials Group, Indira Ghandhi Centre for Atomic Research, Kalpakkam 603102, India
nagesh@igcar.gov.in

[3] Prof. Javier Llorca
IMDEA Materiales, C/ Eric Kandel, 2, Tecnogetafe, 28906 Getafe, Madrid, Spain
javier.llorca@imdea.org

Yours sincerely,

Richard A. Barrett
NUI Galway, Ireland

Highlights

- Net tensile energy governs failure under conventional thermomechanical fatigue.
- Phase angle and dwell periods have a significant effect on fatigue life under TMF.
- Compared with isothermal fatigue, out-of-phase TMF leads to >50% reduction in life.
- In-phase loading is the critical case for TMF with dwell periods at maximum stress.
- Dwell period effects cannot be predicted using empirical life prediction models.

Manuscript (clean and updated version)
Click here to view linked References

Thermomechanical fatigue in 9-12Cr steels: Life prediction models and the effect of tensile dwell periods

Richard A. Barrett[1,2], Christopher J. Hyde[3], Padraic E. O'Donoghue[2,4], Sean B. Leen[1,2]

[1]*Mechanical Engineering, College of Engineering and Informatics, NUI Galway, Galway, H91 HX31, Ireland*
[2]*Ryan Institute for Environmental, Marine and Energy Research, NUI Galway, Galway, H91 HX31, Ireland*
[3]*Department of Mechanical, Materials and Manufacturing Engineering, University of Nottingham, Nottingham NG7 2RD, UK.*
[4]*Civil Engineering, College of Engineering and Informatics, NUI Galway, Galway, H91 HX31, Ireland*

Corresponding Author: Richard A. Barrett
Email: richard.barrett@nuigalway.ie
Tel.: +353 (0)91 492792

Keywords: 9-12Cr steels; Thermo-mechanical fatigue; Dwell periods; Fatigue life prediction

Abstract: This paper is concerned with the assessment of life prediction models for thermomechanical fatigue (TMF), with specific application to P91 steel. A program of TMF tests, including dwell periods, are performed to determine the role of thermomechanical loading on fatigue life. As expected, fatigue life under conventional TMF testing (no dwells) is governed by maximum applied stress and inelastic strain-range. However, with the introduction of dwell periods, at maximum tensile stress during TMF loading, in-phase loading becomes the life-limiting case. This is attributed here to increased microstructural degradation and oxidation, associated with the dwell at peak temperature. Analysis of commonly used TMF life prediction models shows that the effect of dwell periods currently cannot be predicted for in-phase loading. Thus, it is concluded that physically-motivated approaches are required to successfully predict fatigue life under more complex (service) thermomechanical loading histories.

1. Introduction

The transition to highly flexible operation of power plant to accommodate an ever-increasing share of renewable energy technologies on power grids is leading to an increased frequency of complex start-up and shut-down cycles. This cyclic operation of power plant causes severe thermal gradients, especially on thick-walled components, such as header units. At the same time, higher pressures and temperatures are required for increased efficiency and reduced harmful (e.g. CO_2) emissions. Thus, in conjunction with the increased creep and oxidation deformation induced by the higher temperature operating conditions, critical power plant components are now also being subjected to TMF deformation.

9-12Cr steels are key candidate materials for highly flexible operation of heavy-walled components due to (i) high creep strength, (ii) low-cost relative to other materials and (iii) low coefficient of thermal expansion leading to reduced thermal gradients. The high strength of 9-12Cr steels is achieved by a precipitate and solute strengthened martensitic microstructure. The grain structure consists of prior austenite grains (PAGs), packets, blocks and martensitic laths and subgrains in a hierarchical format, which forms due martensitic

transformation during rapid cooling following austenitisation. The 9-12Cr steels are then tempered to improve toughness and to precipitate $M_{23}C_6$ carbides at grain boundaries (GBs) and MX carbonitrides throughout the microstructure.

To date, a range of high temperature low cycle fatigue (HTLCF) test programs have been completed on 9-12Cr steels across a range of temperatures [1-4]. In all experimental work, a Bauschinger effect is observed due to (i) pinning of dislocations at precipitates [5] and (ii) dislocation pile-ups at GBs within the hierarchical microstructure [6], as well as a significant strain-rate effect, particularly at temperatures in excess of 773 K [4,7]. The primary mechanism of degradation under fatigue in 9-12Cr steels is cyclic softening due to recovery of the low-angle boundary (LAB) dislocation substructure [8]. It is well known that this dislocation substructure is critical for enhanced creep strength, with significant reductions in creep rupture time observed for a coarser initial lath microstructure [9] or prior fatigue loading [10]. Hence, cyclic softening leading to accelerated recovery of the LAB microstructure, as observed in fatigue of 9-12Cr steels, can be expected to have a detrimental effect on highly flexible thermomechanical operation of power plant.

A small number of TMF test programs have been conducted to date on 9-12Cr steels [2,11,12], including both in-phase (TMF-IP) and out-of-phase (TMF-OP) loading conditions. Nagesha *et al.* [2] and Saad *et al.* [12] have investigated the effect of different temperature ranges for both TMF-IP and TMF-OP loading conditions in P91 steel, at constant strain-rates of 1.2×10^{-4} s^{-1} and 1.0×10^{-3} s^{-1}, respectively. It is observed that TMF-IP fatigue life is more sensitive to increasing maximum temperature (T_{max}) when compared to TMF-OP test results. This is attributed to enhanced dynamic recovery and creep deformation as T_{max} increases [2]. However, for TMF-OP loading, where a mean tensile stress exists due to the maximum stress coinciding with T_{min}, fatigue lives are found to be consistently lower than the TMF-IP case [2,11,12]. Along with a mean tensile stress, a significant effect of oxide cracking contributes to premature fatigue failure under TMF-OP conditions. The role of coefficient of thermal expansion mismatch between the matrix material and oxide scale is identified as a primary contributor to oxide-assisted cracking under TMF-OP. The mean tensile stress within the oxide scale is relieved via oxide scale cracking, leading to earlier fatigue crack initiation (FCI) under TMF-OP [13].

In TMF tests conducted in the 573 K to 673 K temperature range in P91 steel at a strain-rate of 1.2×10^{-4} s^{-1} [2], dynamic strain aging (DSA) is found to occur. DSA is detected in P91 steel under isothermal conditions in this temperature range also [14]. In terms of higher TMF temperature ranges, DSA is also observed in a RAFM (9Cr-1W-Mn-V-Ta) alloy at a constant strain-rate of 1.2×10^{-4} s^{-1} in the 673 K to 873 K temperature regime once a threshold (accumulated) plastic strain is exceeded, with no DSA observed under isothermal fatigue (IF) conditions in the same temperature interval [15]. Coupled with oxide cracking and mean tensile stress effects, DSA is found to accelerate FCI and crack growth under TMF-OP conditions. However, no DSA (or serrations) is present in TMF testing of P91 steel under the same temperature interval in the 1.2×10^{-4} s^{-1} to 1.0×10^{-3} s^{-1} strain-rate regime [2,12]. It should

also be noted that the above TMF test programs are completed under constant strain-rate, strain-controlled test conditions with a R_ε-ratio ($R_\varepsilon = \varepsilon_{min}/\varepsilon_{max}$) of -1. No TMF test programs on 9-12Cr steels with a R_ε-ratio other than $R_\varepsilon = -1$ have been published to date.

Previous work by this group has presented a significant strain-rate effect in 9-12Cr steels at temperatures in excess of 773 K [4,7] for IF loading conditions. However, as most laboratory IF and TMF tests are conducted under intermediate to higher strain-rates in the 1.0×10^{-2} s^{-1} to 1.0×10^{-4} s^{-1} range, and above the typical service strain-rates of 1.0×10^{-5} s^{-1} to 1.0×10^{-12} s^{-1} in flexible power plant [3,16], it is necessary to understand the effect of strain-rate under TMF conditions. To date, this key effect has not been investigated for 9-12Cr steels and hence, TMF tests at different strain-rates are presented in this study.

Research to date on TMF of 9-12Cr steels identified the critical interactions of creep, TMF and oxidation as key contributors to failure. Fournier and co-workers [17,18,19] have completed a thorough analysis of the interaction of creep, IF and oxidation in 9-12Cr steels, and Gopinath *et al.* [5] conducted an in-depth study of the effect of dwell time, including damage mechanisms, on fatigue life. In terms of creep-TMF (CTMF) testing in an oxidising environment, very little experimental programs have been undertaken to date. Cui and Wang [20] have completed a creep-TMF test program for a simplified service cycle with dwell periods at maximum, minimum and zero strain, including life prediction using a creep-fatigue (CF) modelling framework. Pan *et al.* [21] used strain energy-based life prediction models [22,23] to predict the effect of phase angle on TMF life for phase angles of 0°, 90° and 180° in a P92 steel without dwell periods. However, to the authors knowledge the effect of phase angle on fatigue life of 9-12Cr steels under thermomechanical loading with dwell periods has not been investigated to date. Thus, this study into the effect of dwell periods at phase angles of 0° and 180° on fatigue life of 9-12Cr steels under TMF, critical loading scenarios for current and next generation highly flexible power plant, represents the first such investigation. The role of R_ε-ratio and strain-rate on TMF response are also examined, with the applicability of empirical TMF life prediction models assessed for conventional and asymmetric TMF, as well as CTMF loading conditions.

2. Methodology

2.1. Material and Heat Treatment

The present study is focused on TMF experimental testing of an ex-service P91 tempered-martensite alloy extracted from a superheater outlet header. In service, this material was subjected to subcritical loading conditions only (T_{max} < 758 K) and was removed from service after 35,168 hrs for purely operational reasons, i.e. there was no evidence of any significant material degradation or damage. Thus, negligible creep deformation and microstructural evolution is assumed prior to the current test program. The chemical composition (in wt.%) is 0.007Al-0.1C-8.48Cr-0.42Mn-0.94Mo-0.058N-0.07Nb-0.19Ni-0.013P-0.26Si-0.204V, with

the balance Fe. The P91 steel was fabricated via a rolling process and underwent a typical two-stage heat treatment process of austenitisation at 1323 K for 0.5 hr, followed by tempering at 1038 K for 1 hr.

2.2. Experimental Testing

The high temperature cyclic behaviour of the P91 steel is measured using the Instron 8862 TMF test rig at the University of Nottingham. The test rig and specimen geometry are described in detail elsewhere [24]. The test program includes IF, CF, TMF and CTMF experiments. All tests were performed under strain-control conditions, with the waveforms illustrated schematically in Figure 1. The complete fatigue test program is summarised in Table 1. IF tests are conducted at temperatures of 293 K to 873 K for three different strain-ranges at higher (0.025 to 0.1 %/s) and intermediate (5×10^{-4} %/s) strain-rates. CF tests, with a 120 s dwell period at maximum (tensile) strain, are conducted at temperatures of 673 K, 773 K and 873 K. The TMF and CTMF experiments consist of both in-phase (IP) and out-of-phase (OP) tests with phase angles of 0° and 180°, respectively. The TMF and CTMF experiments are conducted in the 673 K to 873 K temperature range under several strain-ranges in the higher strain-rate regime. Similar to the IF test program, the CTMF test also has a dwell period at maximum tensile strain, corresponding to a dwell at maximum temperature, T_{max}, for IP conditions and at minimum temperature, T_{min}, for OP conditions. Although a dwell period at T_{max} is a commonly used OP cycle, the proposed OP cycle (with a dwell period at T_{min}) is designed to represent part-load operation of power plant. Dwell periods under such conditions occur at a reduced operating temperature similar in magnitude to the T_{min} value of 673 K tested here. Asymmetric TMF tests, where the maximum tensile strain is significantly higher than the maximum compressive strain, were also performed with R_ε-ratios based on predicted strain in the hoop and axial directions for finite element modelling of a header unit under representative (measured) cyclic operation [3]. Thus, the asymmetric TMF tests were performed under IP and OP conditions, with R_ε-ratios of -0.4 and -0.25, representing the upper and lower bounds of the finite element predicted R_ε-ratios. The maximum applied mechanical strain, from 0.3% to 0.5%, is considered important for thermomechanical loading at discontinuities such as welded connections and T-piece connections [25].

A 20% load drop relative to the load at 150 cycles is set as the criterion for test completion. A typical fatigue crack, as observed during the macroscopic fatigue crack growth (FCG) stage of the test, is presented in the optical micrograph of Figure 2. The number of cycles to failure, N_f, is defined via the ISO 12106:2017-03 standard as a 10% drop in load from the secondary softening stage, as illustrated schematically in Figure 3.

2.3. Fatigue life prediction

At present, a number of prominent models exist for predicting LCF life for both IF and TMF loading conditions. In this section, three such models; namely the (i) Coffin-Manson [26,27], (ii) Ostergren [22] and (iii) Zamrik [23] models are assessed for applicability to P91 steel

under the present TMF loading conditions. According to the Coffin-Manson relationship, the number of cycles to failure, N_f, is defined as:

$$N_f = \frac{1}{2}\left(\frac{\Delta\varepsilon_{in}}{2\varepsilon_f'}\right)^{1/c} \quad (1)$$

where ε_f' is the fatigue ductility coefficient and c is the fatigue ductility exponent. The Ostergren model is defined as:

$$N_f = C(\Delta\varepsilon_{in}\sigma_{max})^{\beta} \quad (2)$$

where C and β are the temperature-dependent Ostergren failure parameters. For the Ostergren model here, the inelastic strain energy ($\Delta\varepsilon_{in}\sigma_{max}$) is normalised with respect to the tensile toughness, ΔW_0, to account for temperature-dependence of the Ostergren model failure constants [30], such that the number of cycles to failure is defined as:

$$N_f = C_1\left(\frac{\Delta\varepsilon_{in}\sigma_{max}}{\Delta W_0}\right)^{\beta_1} \quad (3)$$

where C_1 and β_1 are temperature-independent Ostergren failure constants. Similar to the Ostergren model, the Zamrik model is an energy-based life prediction method, specifically proposed to improve TMF-OP life prediction. It is defined as:

$$N_f = C_2\left(\frac{\varepsilon_{ten}\sigma_{max}}{\varepsilon_f\sigma_{UTS}}\right)^{\beta_2} \quad (4)$$

where ε_{ten} is maximum applied tensile stress, ε_f is material ductility, σ_{UTS} is ultimate tensile strength and C_2 and β_2 are the Zamrik parameters.

3. Results

3.1. Cyclic stress-strain response under IF and TMF

Figure 4 presents the measured stress-strain response for the initial cycle of the P91 steel subjected to TMF-IP and TMF-OP loading in the 673 K to 873 K temperature range at an applied strain-rate of 0.025 %/s. The IF response at temperatures of 673 K and 873 K are also included for comparison. As is evident from Figure 4, the TMF response in both cases is effectively bounded by the IF behaviour for both TMF-IP and TMF-OP loading conditions. Figure 5 shows the cyclic stress-strain response for asymmetric loading under a R_ε-ratio of -0.4 for the initial and 100th cycle under TMF-IP loading, with the TMF-OP response presented in Figure 6 at a R_ε-ratio of -0.25. A minimal strain-rate effect is observed under TMF conditions for the higher strain-rate regime considered here. This is due to minimal time spent at 873 K during TMF testing where a significant strain-rate effect is present in P91 steel, with IF test data at less than 773 K demonstrating a negligible strain-rate effect for the higher strain-rates considered here [7].

The measured stress relaxation during the dwell period of the CTMF tests is presented in Figure 7 for both OP and IP loading conditions. A comparison with isothermal CF

experimental data at the dwell temperatures of 673 K and 873 K, respectively, is also presented. To enable a direct comparison of relaxation behaviour across a range of strain-rates, this data is normalised by the stress at the start of the hold period (σ_0). During this isothermal dwell period in the CTMF cycle at the same applied mechanical strain, the observed relaxation of stress in each case is similar to that of the isothermal CF tests at 673 K for the OP case, as presented in Figure 7a. However, there exists a significant difference in relaxation behaviour for dwells at 873 K (Figure 7b). For the strain-rates considered here, no significant strain-rate effect is observed in P91 steel at temperatures below 773 K [7]. However, a significant strain-rate effect is observed in P91 steel under IF at 873 K, as presented in Figure 8a. Thus, it is concluded here that the observed trend in Figure 7b is primarily due to the strain-rate effect under higher dwell temperatures. Figure 8b demonstrates this strain-rate effect as a function of cycles for CTMF-IP thermomechanical loading conditions in the 673 K to 873 K range, where the dwell occurs at 873 K. Once again, the observed cyclic trend for CTMF is consistent with the strain-rate effect observed under IF conditions at 873 K.

The measured evolution of stress range for the CF (at 673 K and 873 K) and CTMF (IP and OP) tests is presented in Figure 9a. As with all tests conducted within this program, significant cyclic softening is observed in all cases, with only slight differences in the level and rate of softening between CTMF-IP and CTMF-OP loading conditions. Figure 9b presents the accumulated inelastic strain, $p = 2\sum_{\mathrm{i}=1}^{N_\mathrm{f}} \Delta\varepsilon_{\mathrm{in,i}}$, where N_f is the number of cycles to failure and $\Delta\varepsilon_{\mathrm{in,i}}$ is inelastic strain range for cycle i, as defined in Figure 10 for CTMF-IP and CTMF-OP loading and comparisons with the corresponding CF data at 673 K and 873 K. The results for CTMF-IP and CTMF-OP suggests a strong dependence of cyclic softening on p, as opposed to temperature, for tests conducted below 873 K. As the primary mechanism of cyclic softening in 9-12Cr steels is LAB dislocation annihilation [8], the hypothesis that cyclic softening is predominantly a function of p is consistent with published observations of negligible LAB evolution under thermal aging conditions [28]. This dependence on p is further realised via the application of Chaboche isotropic stress model to cyclic softening in P91 by Saad *et al.* [12].

3.2. Failure under TMF conditions

Figure 11 presents the effect of symmetric thermomechanical loading (TMF-IP and TMF-OP) on fatigue life as a function of both applied mechanical strain-range and inelastic strain range, $\Delta\varepsilon_{\mathrm{in}}$, for P91 steel, including a comparison with IF data. Clearly, thermal cycling leads to a significant reduction in fatigue life, compared with isothermal loading. For symmetric TMF, the most severe case is the TMF-OP case. As the mechanical strain and temperature are out-of-phase, the material is subjected to a significantly higher maximum tensile stress (see Figure 12a) at minimum temperature. This is essentially due to the material reaching a higher maximum stress at the lower temperature (under strain control conditions) and giving a harder response (since maximum tensile stress is a key parameter for FCI). This result

demonstrates the critical role of maximum applied tensile stress, σ_{max}, on fatigue life for symmetric TMF. It should also be noted that there is a significant temperature-dependence for the number of cycles to failure as a function of the applied mechanical strain-range for IF conditions (Figure 11a). However, this temperature-dependence is not as evident when considering inelastic strain-range versus N_f, where the IF test data essentially collapses to a power law relationship as shown in Figure 11b.

Figure 11 also presents a comparison of the observed fatigue life of asymmetric TMF-IP and TMF-OP test results (open symbols). As is evident from this result, the asymmetric TMF tests follow the same trend (qualitatively) as symmetric TMF tests (TMF-OP has reduced fatigue life compared with TMF-IP), albeit under a significantly different relationship with inelastic strain-range for TMF-IP for the strain-ranges considered here. This may represent the transition from low-cycle fatigue to high-cycle fatigue for P91 steel. Thus, further testing at these lower applied strain-ranges under IF and TMF (both symmetric and asymmetric) test conditions is required to define whether this is the transition region for low-cycle fatigue to high-cycle fatigue; this will also provide essential data for plant designers and fatigue life prediction at these potentially crucial strain-ranges for conventional power plant applications.

TMF-OP is similar to isothermal CF (dwell) loading, in which the inelastic strain accumulation is dominant in the compressive part of the loop [13]. The net effect is a mean tensile stress (e.g. see Figure 12b) and hence, reduced fatigue life compared with TMF-IP and IF test data, as illustrated in Figure 11. However, as shown in Figure 13, a significant increase in fatigue life is observed for OP loading with a tensile dwell period (CTMF-OP) when, compared with CTMF-IP test data. This phenomenon is not captured by the mean stress or maximum applied stress effect. This contrasts with the finding for TMF tests without a hold period and highlights (i) the significance of high temperature creep-TMF-oxidation deformation in P91 steels, (ii) the requirement to conduct TMF tests with dwell periods for highly flexible power plant applications and (iii) the requirement to assess current TMF life prediction methodologies for cases of asymmetric TMF and TMF with dwell periods.

3.3. The concept of net tensile hysteresis energy and CTMF behaviour

The net tensile hysteresis energy (ΔW_T) is widely used to evaluate fatigue life [2,29] and is defined schematically in Figure 10 for a CF loading case. Inelastic strain range, $\Delta\varepsilon_{in}$, represents the primary mechanism of energy dissipation at high applied (tensile) stresses, with the dissipated energy predominantly absorbed by the material (the remainder is dissipated as heat to the surroundings). Thus, increasing ΔW_T is nominally consistent with a decreasing fatigue life. Figure 14 presents the measured ΔW_T for TMF-IP and TMF-OP under an applied mechanical strain range of ±0.5% and strain-rate of 0.025 %/s. The ΔW_T is evaluated based on the half-life tensile hysteresis loop area. A significant increase in ΔW_T is observed for the TMF-OP test conditions compared with TMF-IP due to the increased applied stress associated with the reduced temperature during tensile loading. This increase in

ΔW_T is consistent with a decrease in fatigue life. Furthermore, qualitatively, the ΔW_T approach is capable of predicting the observed trend of reduced fatigue life for TMF-OP loading conditions as compared with TMF-IP (e.g. see Figure 14). However, the correlation of N_f with ΔW_T is not valid for CTMF loading conditions. As illustrated in Figure 14, both ΔW_T and fatigue life increase for CTMF loading conditions relative to the corresponding TMF conditions. This is inconsistent with the observed TMF trend that increasing ΔW_T reduces the fatigue life.

3.4. Calibration of fatigue life prediction models for TMF of P91 steel

To apply the Coffin-Manson model to TMF loading in the 673 K to 873 K temperature range, the necessary failure constants (ε_f' and c) are defined using IF data for 673 K, 773 K and 873 K. As is evident in Figure 15a, the data for the three temperatures collapses to approximately a linear relationship for $\Delta\varepsilon_{in}/2$ versus N_f on a log-log plot, with $\Delta\varepsilon_{in}$ taken as the inelastic strain range at half-life. However, as illustrated in Figure 15b, when the same constants are used for TMF loading, the Coffin-Manson relationship predicts extremely non-conservative TMF life compared with experimental data. For the temperature ranges and test conditions considered here, Coffin-Manson is shown to be non-conservative by factors of approximately 6 and 12 for TMF-IP and TMF-OP cases, respectively. This is primarily attributed to the omission of a maximum stress component, an important parameter for TMF life prediction (e.g. see Figure 12a), from the model.

The value of ΔW_0 for P91 steel is identified from monotonic tensile testing of the material [31] and presented in Table 2. The identified failure constants, C_1 and β_1, are 10.57 and -1.44, respectively (see Figure 16a). Figure 16b presents application of the Ostergren model to P91 steel under IF and TMF loading conditions. For TMF loading, $\Delta\varepsilon_{in}\sigma_{max}$, taken at the half-life here, is normalised with respect to ΔW_0 at the maximum cycle temperature (873 K here). As is evident from Figure 16b, extrapolation of the Ostergren model to TMF using failure constants identified from IF data gives non-conservative results, particularly for TMF-OP. If the Ostergren model is normalised with respect to ΔW_0 at the mean temperature (773 K here), the predicted TMF lives are far less conservative. Thus, it is recommended that the Ostergren model be applied with normalisation to ΔW_0 at maximum temperature and that the Ostergren model not be used for TMF-OP loading conditions in 9-12Cr steels.

In Equation (4), $\varepsilon_{ten}\sigma_{max}$ is determined from the half-life hysteresis loop and ε_f and σ_{UTS} are determined from tensile test data as presented in Table 2. Figure 17a presents identification of the temperature-dependent failure constants, C_2 and β_2, from IF data and Figure 17b compares the predicted number of reversals to failure with experimentally observed values for the IF and symmetric TMF cases. The Zamrik model is utilised here with ε_f and σ_{UTS} defined at the maximum temperature, as application at the mean temperature leads to non-conservative results. Although the Zamrik model predicts N_f of symmetric tests quite well (see Figure 17b), this model struggles to predict the fatigue life of (i) asymmetric TMF cycles for the

strain-ranges considered here, as presented in Figure 18a, where results are conservative for the TMF-IP case, and (ii) more importantly, CTMF-IP loading in Figure 18b, where non-conservative results by a factor of approximately 4 are predicted.

4. Discussion

The strain-life failure for symmetric TMF-IP and TMF-OP loading conditions in Figure 11 is consistent with the key roles of maximum tensile stress, σ_{max}, and mean stress, σ_m, in determining fatigue life. Under such loading conditions, ΔW_T can be generally used to correlate fatigue life with life prediction models based on ΔW_T, such as Ostergren (TMF-IP only) and Zamrik. A key benefit of such models is that they can be implemented in multi-axial form in conjunction with critical plane and rainflow cycle counting methods for application to realistic geometries [3,32]. Based on the results of Figure 15 to Figure 17, the Zamrik model performs best for prediction of TMF life, particularly for TMF-OP, whereas the Ostergren model gives significantly non-conservative results. For the Ostergren and Zamrik models, using the maximum temperature as the reference temperature leads to increased conservatism of life prediction. It should also be noted here that the analysis performed does not account for the effect of strain-rate on the mechanical properties and failure constants within the life prediction models; future work should address this effect for strain-rates observed in conventional plant (e.g. 1×10^{-5} s^{-1} to 1×10^{-12} s^{-1}) as $\Delta\varepsilon_{in}$, σ_{max} and σ_{UTS}, for example, depend on strain-rate.

The symmetric TMF test results follow the typical phenomenon of reduced fatigue life for TMF-OP loading compared to TMF-IP (e.g. see Figure 11), with failure driven by a mean tensile stress, as highlighted in Figure 12b. However, the CTMF test program on P91 steel conducted here highlights a contrasting trend, with CTMF-IP loading giving lower fatigue life than the CTMF-OP cases. For CTMF-IP cases considered here, the 120 s dwell period at maximum tensile strain occurs at the maximum temperature of 873 K, where increased microstructural degradation and creep deformation occur. However, for the CTMF-OP case, the dwell period occurs at low temperature, where rate effects and creep deformation are significantly reduced. Furthermore, increased oxidation during a dwell period at higher temperature under CTMF-IP will lead to increased oxide-scale contribution to FCI and hence, reduced fatigue life. Earthman *et al.* [33] have demonstrated this significant effect of oxidation on IF life, and in particular for FCI, in a 12Cr steel. This reduced fatigue life can be attributed to the mechanisms of oxide layer rupture under cyclic mechanical loading [11,13,34], in which rupture of the outermost oxide scale reveals fresh matrix material on which an oxide-scale rapidly forms, with the process repeating until oxide-scale assisted FCI and premature failure occur. As the oxide-scale thickness, h_{ox}, is a function of the temperature-dependent diffusion constant, $D(T)$, i.e. following a parabolic growth law, $h_{ox} = \sqrt{D(T)t}$, the higher dwell temperature of the CTMF-IP test condition will induce increased and accelerated oxide scale growth and, hence, reduced cycles to FCI, as compared with the CTMF-OP case. Thus, for CTMF-IP tests conducted with a dwell period at higher

temperature, the role of oxide scale formation and evolution of the oxide scale on FCI needs to be investigated in more detail for CTMF loading conditions.

As illustrated in Figure 12, the observed TMF-OP and CTMF-OP fatigue lives are quite similar, demonstrating the minimal effect of the 120 s dwell period on fatigue life at 673 K. This is consistent with minimal creep and oxidation damage at temperatures less than 773 K in P91 steels. Thus, it can be concluded that higher temperature dwell periods, e.g. where strain-rate effects and temperature-dependent microstructural degradation become important, can have a detrimental effect on fatigue life. Although conventional power plant components tend to operate with dwell periods on the order of hours, a significant proportion of the thermal stress component relaxes during the initial (rapid) stage of a hold period. For 9-12Cr steels, this initial stage of stress relaxation is on the order of minutes with the stress rapidly decaying to a saturated value [4]. Hence, the 120 s dwell period considered here can qualitatively capture the relaxation behaviour of P91 steel. However, future work will also investigate the effect of dwell time on CF and CTMF performance in 9-12Cr steels to determine the role of microstructural degradation during dwell periods on fatigue life. As the proposed TMF life prediction models follow the trend of reduced fatigue life for increased $\Delta\varepsilon_{in}$ and mean applied stress, these models are not readily applicable to CTMF. Hence, as such dwell periods will become ever more commonplace for current and next generation plant service loading conditions, a fatigue life prediction model which accounts for interactions of creep, TMF and oxidation mechanisms of degradation and FCI is required as the models presented here do not account for microstructural degradation, creep and, potentially most importantly, oxidation effects. For example, Wei *et al.* [35] developed a probabilistic linear superposition crack growth model for creep-fatigue-oxidation during system start-up and shut-down and for 9-12Cr steels, Fournier and co-workers [19] applied a Tanaka-Mura FCI model coupled with crack growth to creep-fatigue-oxidation. Furthermore, the key life limiting factor for 9-12Cr steels under high temperature operation is microstructural degradation, including precipitate coarsening, formation of secondary phase particles (such as Laves phase and Z-phase particles at the expense of solute atoms and carbonitride particles), oxide-scale formation and dynamic recovery. This microstructural degradation, which is dependent on thermal and mechanical loading history, can lead to a significant reduction in strength and the formation of micro-voids [36] and micro-cracks [32], potentially leading to material failure. Thus, microstructure evolution under complex thermomechanical cycles, and its effect on material behaviour, should represent a critical constituent in life prediction and remnant life analysis of power plant components, particularly as higher temperature flexible operation is being pursued. This is even more important in terms of the heterogeneous microstructure of welded connections and their susceptibility to premature failure. Thus, constitutive models should account for the complete array and interdependencies of strengthening mechanisms in 9-12Cr steels [37] and complex microstructural evolution under creep-TMF-oxidation (e.g. significant effect of prior fatigue loading on creep performance of P92 [10]).

5. Conclusions

A program of TMF tests on a P91 steel are presented and current empirical fatigue life prediction models are assessed for applicability to 9-12Cr steels. The key conclusions are:

- In the 673 K to 873 K temperature range considered here, out-of-phase thermomechanical loading is observed to cause a significant reduction in life compared with isothermal fatigue and in-phase thermomechanical fatigue. In such cases, the fatigue life is strongly influenced by the maximum tensile stress.
- When dwell periods are introduced at maximum tensile stress, in-phase loading becomes the critical loading case due to microstructure evolution and accelerated oxide scaling during dwells at peak temperature. This highlights the necessity to complete creep-thermomechanical fatigue testing and the requirement to consider the physical mechanisms of fatigue crack initiation under combined creep, thermomechanical fatigue and oxidation loading conditions.
- Conventional thermomechanical fatigue life prediction models based on inelastic strain energy (e.g. Ostergren and Zamrik) should be used with caution for 9-12Cr steels; such models break down for cases where thermomechanical fatigue loading with high temperature dwell periods.
- Physically-motivated approaches are required to successfully predict fatigue life under complex (service) thermomechanical loading histories. Such approaches must account for microstructural evolution, as well as plasticity- and oxidation-induced mechanisms of fatigue crack initiation.

Acknowledgements

This publication has emanated from research conducted with the financial support of Science Foundation Ireland under Grant Number SFI/14/IA/2604. The authors would also like to acknowledge the contributions made by the collaborators of the MECHANNICS project, including Prof Noel O'Dowd of the University of Limerick.

References

1. Fournier, B., Dalle, F., Sauzay, M., Longour, J., Salvi, M., Caës, C., Tournié, I., Giroux, P.-F., Kim S.-H. Comparison of various 9-12%Cr steels under fatigue and creep-fatigue loadings at high temperature. *Materials Science and Engineering A*, **528** (2011) 6934-6945.
2. Nagesha, A., Kannan, R., Sastry, G.V.S., Sandhya, R., Singh, V., Bhanu Sankara Rao, K. Isothermal and thermomechanical fatigue studies on a modified 9Cr-1Mo ferritic martensitic steel. *Materials Science and Engineering A*, **554** (2012) 95-104.
3. Farragher, T.P., Scully, S., O'Dowd, N.P., Leen, S.B. Development of life assessment procedures for power plant headers operated under flexible loading scenarios. *International Journal of Fatigue*, **49** (2013) 50-61.
4. Barrett, R.A., O'Hara, E.M., O'Donoghue, P.E., Leen, S.B. High temperature low cycle fatigue behaviour of MarBN at 600 °C. *Transactions ASME Journal of Pressure Vessel Technology.*, **138** (2016) 041401.
5. Gopinath, K., Gupta, R.K., Sahu, J.K., Ray, P.K., Ghosh, R.N. Designing P92 grade martensitic steel header pipes against creep-fatigue interaction loading condition: Damage micromechanisms. *Materials and Design*, **86** (2015) 411-420.
6. Chauhan, A., Litvinov, D., de Carlan, Y., Aktaa, J. Study of the deformation and damage mechanisms of a 9Cr-ODS steel: Microstructure evolution and fracture characteristics. *Materials Science and Engineering A*, **658** (2016) 123-134.
7. Barrett, R.A., O'Donoghue, P.E., Leen, S.B. A dislocation-based model for high temperature cyclic viscoplasticity of 9-12Cr steels. *Computational Materials Science*, **92** (2014) 286-297.
8. Sauzay, M., Fournier, B., Mottot, M., Pineau, A., Monnet, I. Cyclic softening of martensitic steels at high temperature - experiments and physically-based modelling. *Materials Science and Engineering A*, **483-484** (2008) 410-414.
9. Ennis, P.J., Zielinska-Lipiec, A., Wachter, O., Czyrska-Filemonowicz, A. Microstructural stability and creep rupture strength of the martensitic steel P92 for advanced power plant. *Acta Materialia*, **45** (1997) 4901-4907.
10. Zhang, W., Wang, X., Gong, J., Jiang, Y., Huang, X. Experimental and simulated characterization of creep behaviour of P92 steel with prior cyclic loading damage. *Journal of Materials Science and Technology*, **33** (2017) 1540-1548.
11. Mannan, S.L., Valsan, M. High-temperature low cycle fatigue, creep-fatigue and thermomechanical fatigue of steels and their welds. *Int. J. Mech. Sciences*, **48** (2006) 160-175.
12. Saad, A.A., Hyde, C.J., Sun, W., Hyde, T.H. Thermal-mechanical fatigue simulation of a P91 steel in a temperature range of 400-600 °C. *Materials at High Temperature*, **28** (2011) 212-218.

13. Nagesha, A., Kannan, R., Sandhya, R., Sastry, G.V.S., Mathew, M.D., Bhanu Sankara Rao, K., Singh, V. Thermomechanical fatigue behaviour of a modified 9Cr-1Mo ferritic-martensitic steel. *Procedia Engineering*, **55** (2013) 199-203.
14. Keller, C., Marguiles, M.M., Hadjem-Hamouche, Z., Guillot, I. Influence of the temperature on the tensile behaviour of a modified 9Cr-1Mo T91 martensitic steel. *Materials Science and Engineering A*, **527** (2010) 6758-6764.
15. Nagesha, A., Kannan, R., Srinivasan, V.S., Parameswaran, P., Sandhya, R., Choudhary, B.K., Mathew, M.D., Jayakumar, T., Rajendra Kumar, E. Thermomechanical fatigue behaviour of a reduced activation ferritic-martensitic steel. *Procedia Engineering*, **86** (2014) 88-94.
16. Nabarro, F. Creep at very low rates. *Metallurgical and Materials Transactions A*, **33** (2002) 213-218.
17. Fournier, B., Sauzay, M., Caës, C., Noblecourt, M., Mottot, M., Bougault, A., Rabeau, V., Pineau, A. Creep-fatigue-oxidation interactions in a 9Cr-1Mo martensitic steel. Part I: Effect of tensile holding period on fatigue lifetime. *International Journal of Fatigue*, **30** (2008) 649-662.
18. Fournier, B., Sauzay, M., Caës, C., Noblecourt, M., Mottot, M., Bougault, A., Rabeau, V., Pineau, A. Creep-fatigue-oxidation interactions in a 9Cr-1Mo martensitic steel. Part II: Effect of compressive holding period on fatigue lifetime. *International Journal of Fatigue*, **30** (2008) 663-676.
19. Fournier, B., Sauzay, M., Caës, C., Noblecourt, M., Mottot, M., Bougault, A., Rabeau, V., Pineau, A. Creep-fatigue-oxidation interactions in a 9Cr-1Mo martensitic steel. Part III: Lifetime prediction. *International Journal of Fatigue*, **30** (2008) 1797-1812.
20. Cui, L., Wang, P. Two lifetime estimation models for steam turbine components under thermomechanical creep-fatigue loading. *International Journal of Fatigue*, **59** (2014) 129-136.
21. Pan, X.-M., Li, X., Chang, L., Zhang, G.-D., Xue, F., Zhao, Y.-F., Zhou, C.-Y. Thermal-mechanical fatigue behaviour and lifetime prediction of P92 steel with different phase angles. *International Journal of Fatigue*, **109** (2018) 126-136.
22. Ostergren, W.J. A damage function and associated failure equations for predicting hold time and frequency effects in elevated temperature, low cycle fatigue. *Journal of Testing and Evaluation*, **4** (1976) 327-339.
23. Zamrik, S.Y., Renauld, M.L. Thermo-mechanical out-of-phase fatigue life of overlay coated IN-738LC gas turbine material. *ASTM Special Publication*, **1371** (2000) 119-137.
24. Hyde, C.J., Sun, W., Leen, S.B. Cyclic thermo-mechanical material modelling and testing of 316 stainless steel. *International Journal Pressure Vessel and Piping*, **87**, (2010) 365-372.
25. Li, M., Barrett, R.A., Scully, S., Harrison, N.M., Leen, S.B., O'Donoghue, P.E. Cyclic plasticity of welded P91 material for simple and complex power plant connections. *International Journal of Fatigue*, **87** (2016) 391-404.

26. Coffin, L.F. A study of the effects of cyclic thermal stresses on a ductile metal. *Transactions of ASME*, **76** (1954) 931-950.
27. Manson, S.S. Behaviour of materials under conditions of thermal stress. *NACA Report 1170*, Lewis Flight Propulsion Laboratory: Cleveland (1953).
28. Panait, C.G., Zielińska-Lipec, A., Koziel, T., Czyrska-Filemonowicz, A., Gourgues-Lorenzon, A.-F., Bendick, W. Evolution of dislocation density, size of subgrains and MX-type precipitates in a P91 steel during creep and during thermal ageing at 600 °C for more than 100,000 h. *Materials Science and Engineering A*, **527** (2010) 4062-4069.
29. Song, G., Hyun, J., Ha, J. Creep-fatigue life prediction of aged 13CrMo44 steel using the tensile plastic strain energy. In: Rémy, L., Petit, J. (Eds.) Temperature-Fatigue Interaction. Elsevier Applied Science: London (2002) 65-73.
30. Lee, K.-O, Hong, S.-G., Lee, S.-B. A new energy-based fatigue damage parameter in life prediction of high temperature structural materials. *Materials Science and Engineering A*, **496** (2008) 471-477.
31. Golden, B.J., Li, D.-F., Tiernan, P., Scully, S., O'Dowd, N.P. Deformation characteristics of a high chromium power plant steel at elevated temperatures. *Proceedings of the ASME 2015 Pressure Vessel and Piping Conference (PVP2015)*, Boston, Massachusetts, USA, July 19th - 23rd, 2015.
32. O'Hara, E.M., Harrison, N.M., Polomski, B.K., Barrett, R.A., Leen, S.B. The effect of inclusions on the high-temperature low-cycle fatigue performance of cast MarBN: Experimental characterisation and computational modelling. *Fatigue and Fracture of Engineering Materials and Structures*, **41** (2018) 2288-2304.
33. Earthman, J.C., Eggeler, G., Ilschner, B. Deformation and damage processes in a 12%Cr-Mo-V steel under high temperature low cycle fatigue conditions in air and vacuum. *Materials Science and Engineering A*, **110** (1989) 103-114.
34. Neu, R.W., Sehitoglu, H. Thermomechanical fatigue, oxidation and creep: Part I. Damage mechanisms. *Metallurgical Transactions A*, **20** (1989) 1755-1767.
35. Wei, Z., Yang, F., Lin, B., Luo, L., Konson, D., Nikbin, K. Deterministic and probabilistic creep-fatigue-oxidation crack growth modelling. *Probabilistic Engineering Mechanics*, **33** (2013) 126-134.
36. Pandey, C., Saini, N., Mahapatra, M.M., Kumar, P. Study of the fracture surface morphology of impact and tensile tested cast and forged (C&F) Grade 91 steel at room temperature for different heat treatment regimes. *Engineering Failure Analysis*, **71** (2017) 131-147.
37. Barrett, R.A., O'Donoghue, P.E., Leen, S.B. A physically-based high temperature yield strength model for 9Cr steels. *Materials Science and Engineering A*, **730** (2018) 410-424.

Tables

Table 1: High temperature cyclic test program on P91 steel.

Test Type	***Temperature* (K)**	***Strain range* (%)**	***Strain-rate* (%/s)**	***Waveform***
IF	293, 673, 773 and 873	±0.5 ±0.5 ±0.4 ±0.3 ±0.5	0.1 0.033 0.033 0.033 0.025	R_ε = -1 (Triangular)
IF	673, 773, 823, 873 and 898	±0.3	5×10^{-4}	R_ε = -1 (Triangular)
CF	673, 773 and 873	±0.3	0.1	120 s hold period (Triangular)
TMF (IP & OP)	673 to 873	±0.5 ±0.5 ±0.5 ±0.4 ±0.3	0.033 0.025 0.01 0.033 0.033	R_ε = -1 (Triangular)
TMF (IP & OP)	673 to 873	+0.5,-0.2 +0.5,-0.2 +0.4,-0.1 +0.4,-0.1 +0.4,-0.1	0.033 0.025 0.033 0.025 0.01	R_ε = -0.4; R_ε = -0.25 Asymmetric (Triangular)
CTMF (IP & OP)	673 to 873	±0.5	0.033 0.025	120 s hold period (Triangular)

Table 2: Measured monotonic properties of P91 steel for Ostergren and Zamrik models.

T (K)	ΔW_0 (MJ/m^3)	σ_{UTS} (MPa)	ε_f (%)
293	109	690.2	17.9
673	78	612.0	25
773	71	530.0	16.2
873	43	391.4	18.7

Figures

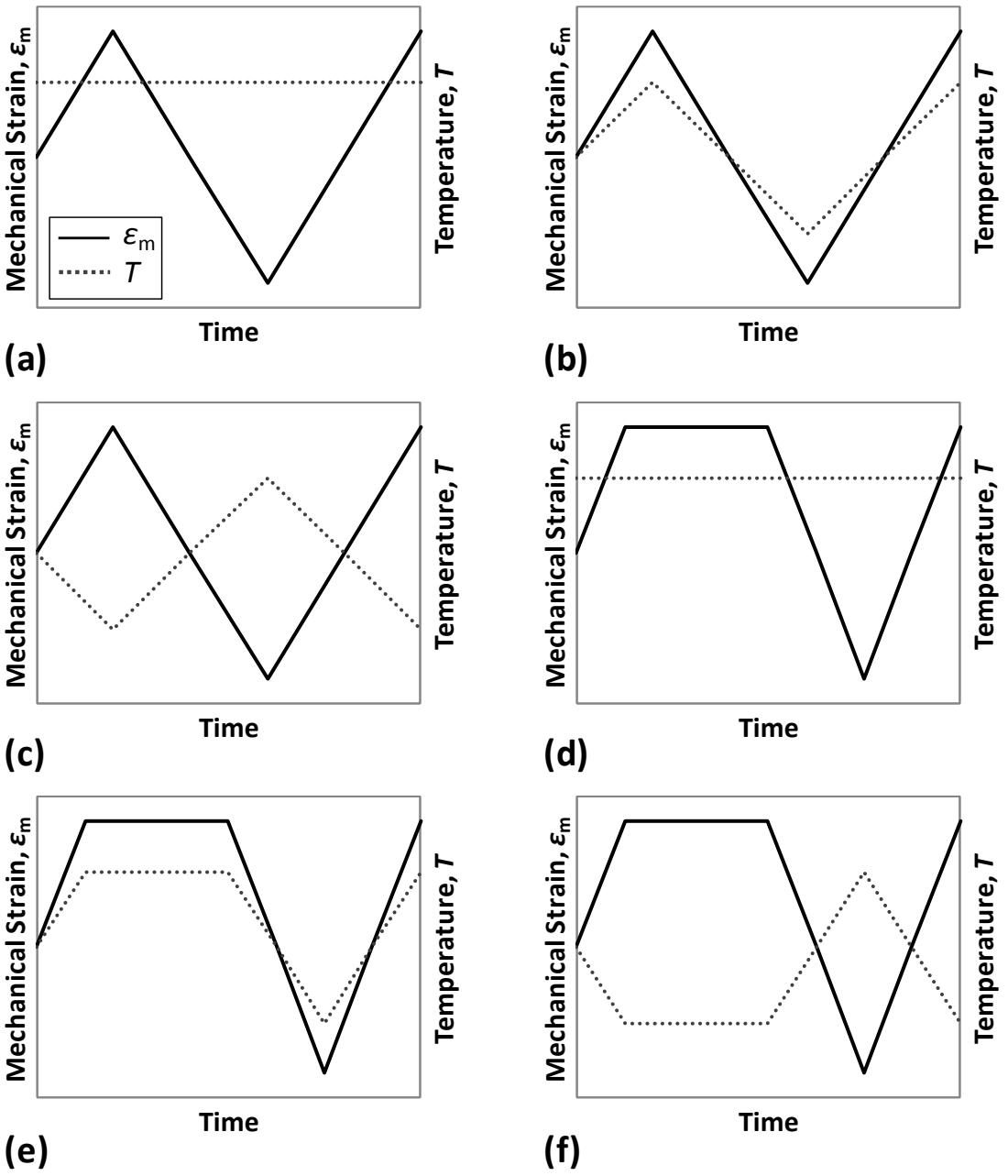

Figure 1: IF, TMF and CTMF waveforms in the test program: (a) IF, (b) TMF-IP, (c) TMF-OP, (d) CF, (e) CTMF-IP and (f) CTMF-OP.

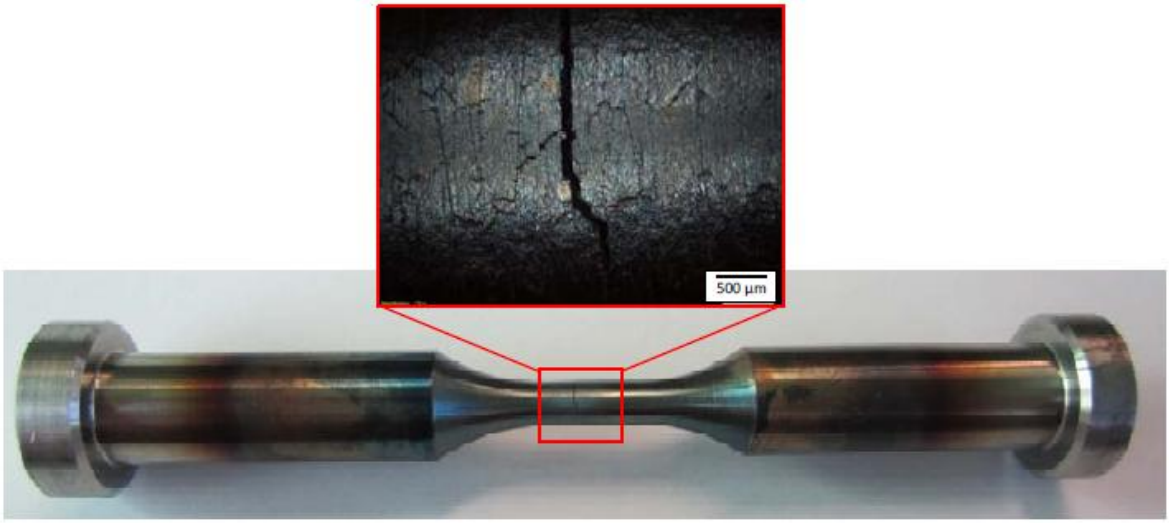

Figure 2: TMF specimen post-test and optical micrograph of the dominant fatigue crack under a failure criterion of a 20% drop in load after 150 cycles (inset).

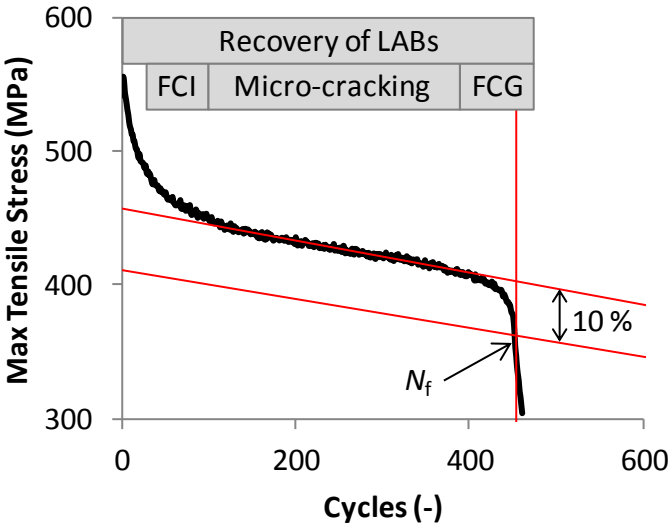

Figure 3: Cyclic softening of P91 steel under TMF-IP loading with deformation mechanism map highlighting recovery (lath widening and particle coarsening), fatigue crack initiation (FCI), coalescence to form micro-cracks and macroscopic fatigue crack growth (FCG).

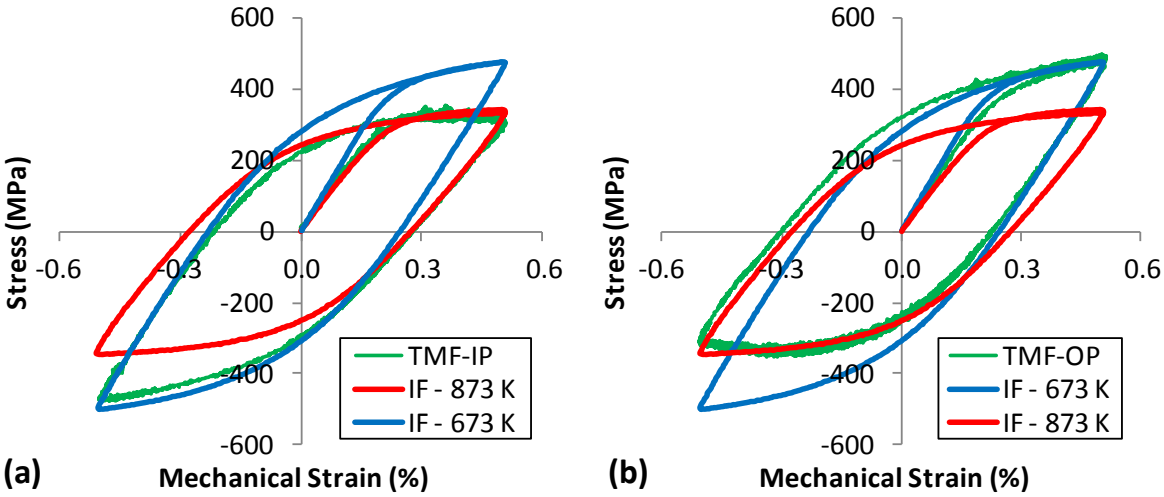

Figure 4: Comparison of (a) TMF-IP and (b) TMF-OP cyclic stress-strain response with IF data at 673 K and 873 K for the initial cycle at an applied strain-rate of 0.025 %/s and mechanical strain-range of ±0.5%.

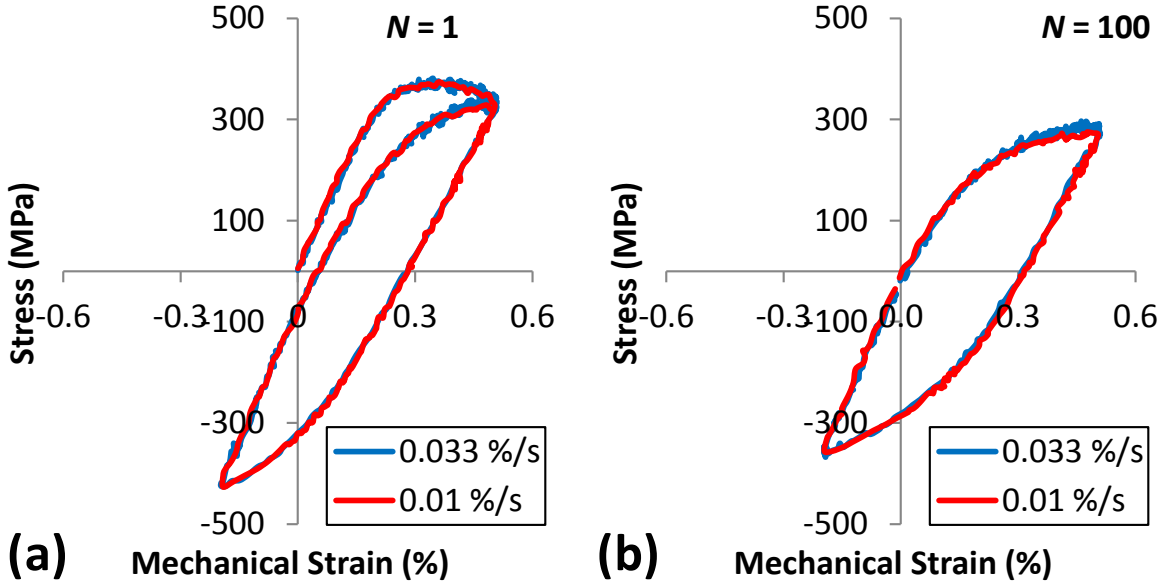

Figure 5: TMF-IP behaviour of P91 steel under asymmetric TMF testing for the (a) initial and (b) 100th cycle in the 673 K to 873 K temperature range under a R_ε-ratio of -0.4.

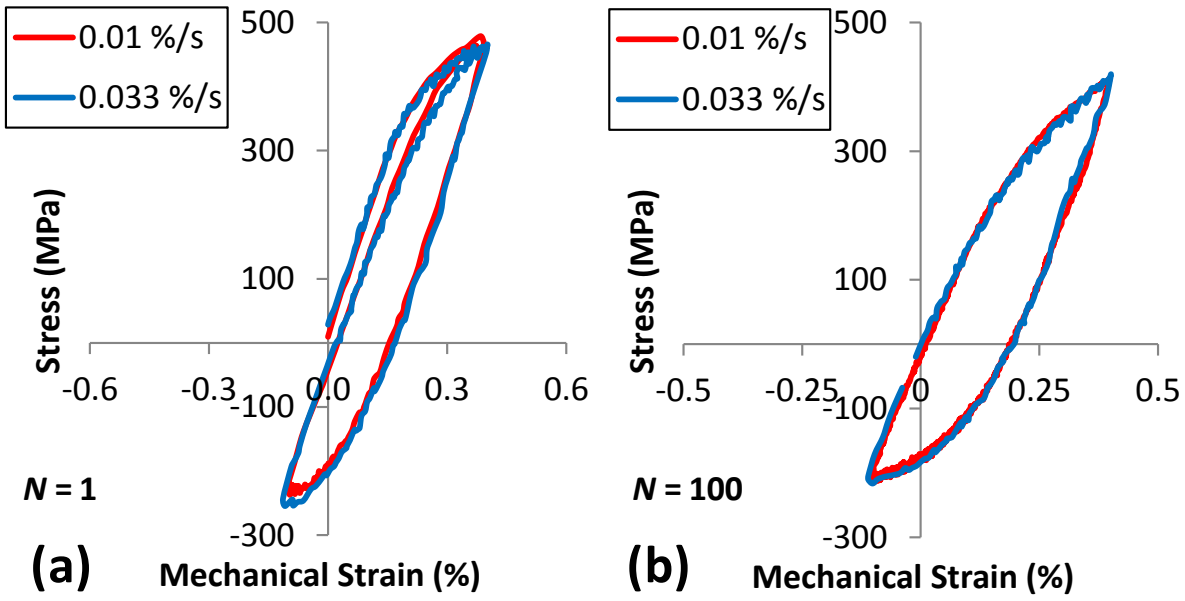

Figure 6: TMF-OP behaviour of P91 steel under asymmetric TMF testing for the (a) initial and (b) 100th cycle in the 673 K to 873 K temperature range under a R_ε-ratio of -0.25.

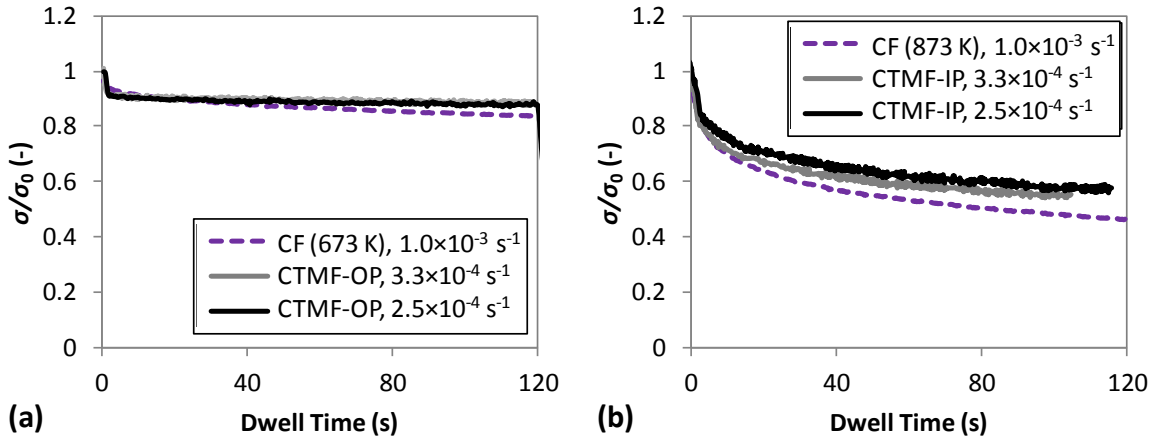

Figure 7 Comparison of the measured (a) CTMF-OP and (b) CTMF-IP stress response during the dwell period (solid lines) for two different strain-rates of 3.3×10^{-4} s^{-1} and 2.5×10^{-4} s^{-1}. A comparison with isothermal CF experimental data at the dwell temperature is also included (dotted lines) at an alternate strain-rate of 1.0×10^{-3} s^{-1}. The stress values are normalised with respect to the initial stress at the start of the hold period. The applied mechanical strain during the dwell period is 0.5% in all cases.

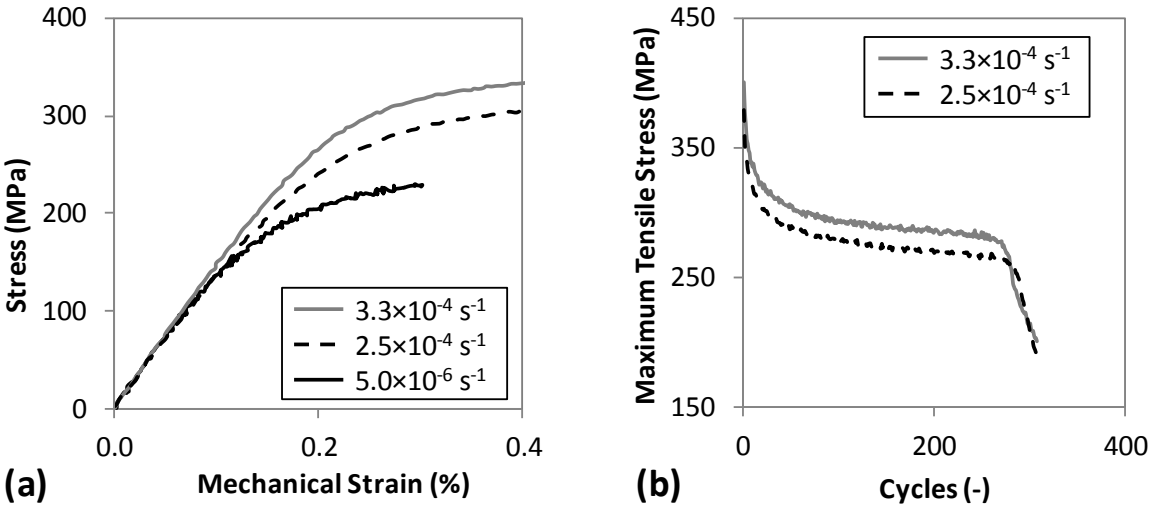

Figure 8: Effect of strain-rate on (a) tensile stress-strain response under IF loading at 873 K and (b) evolution of maximum tensile stress with increasing cycles under CTMF-IP loading.

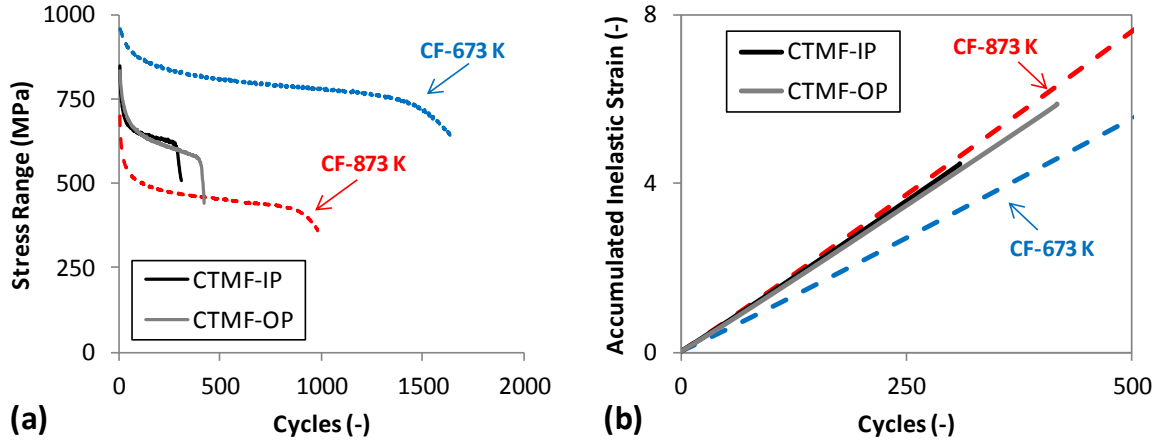

Figure 9: Measured cyclic evolution of (a) stress range and (b) accumulated effective inelastic strain for CF (dashed lines) and CTMF (IP and OP, solid lines) test conditions in the 673 K to 873 K temperature range.

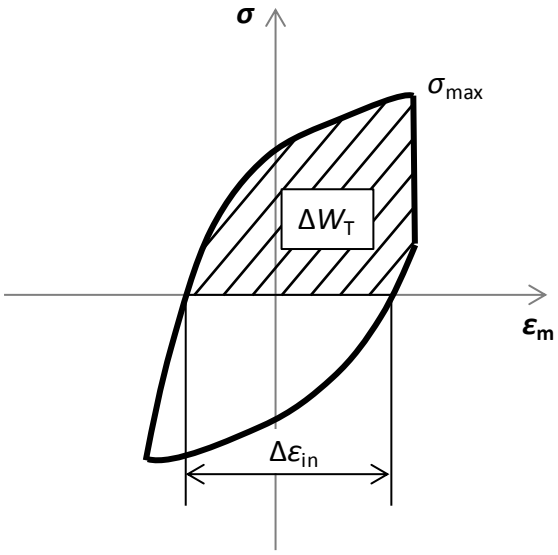

Figure 10: Schematic representation of the net tensile hysteresis energy in a CF test.

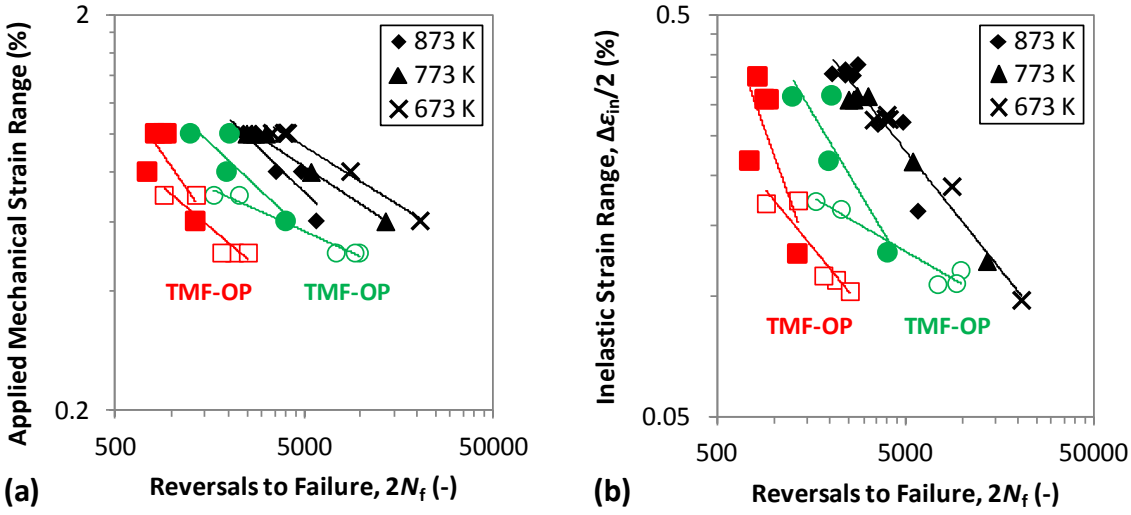

Figure 11: Number of reversals to failure as a function of (a) total applied strain-range and (b) inelastic strain-range for IF (673 K, 773 K and 873 K) and TMF-IP and TMF-OP in the 673 K to 873 K temperature range. Symmetric TMF results are in full symbols and asymmetric TMF test results are in open symbols.

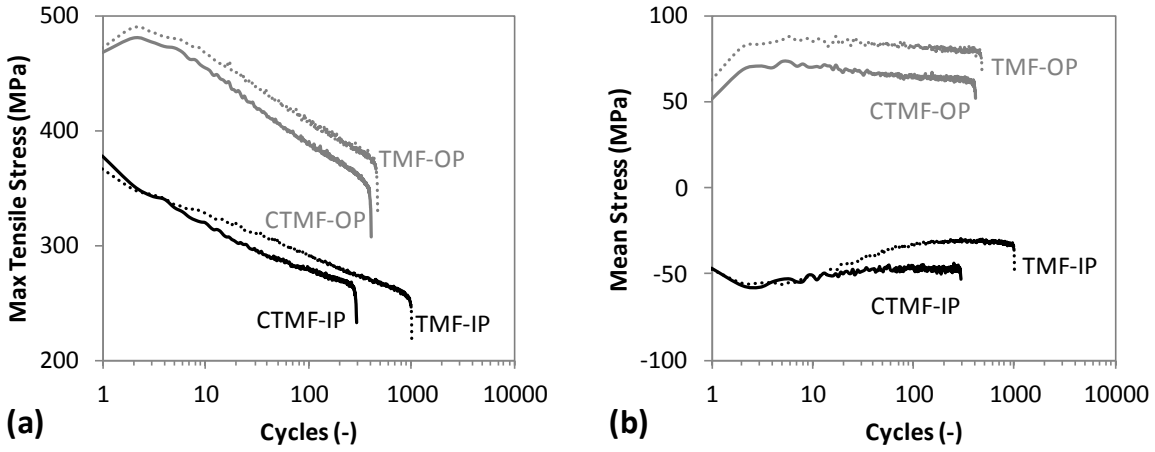

Figure 12: Cyclic evolution of (a) maximum tensile stress and (b) mean stress for TMF and CTMF loading under IP and OP thermo-mechanical conditions. The strain-rate is 0.025 %/s and applied mechanical strain is ±0.5%.

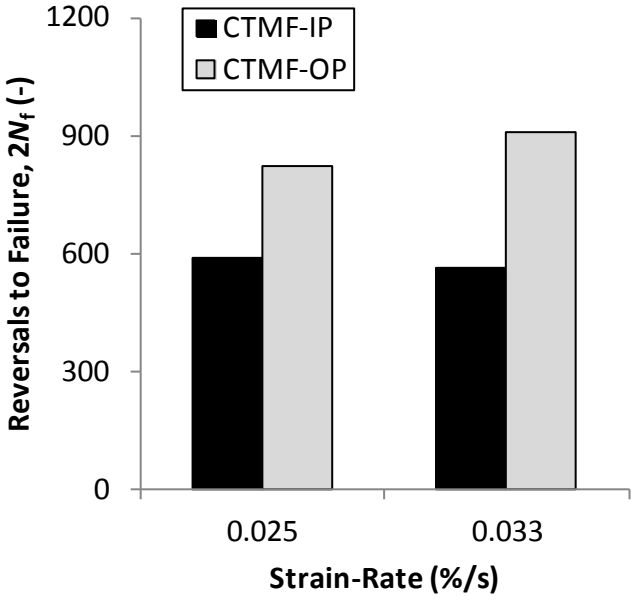

Figure 13: Increased reversals to failure associated with CTMF-OP loading condition compared with CTMF-IP behaviour for an applied mechanical strain is ±0.5% at two different strain-rates.

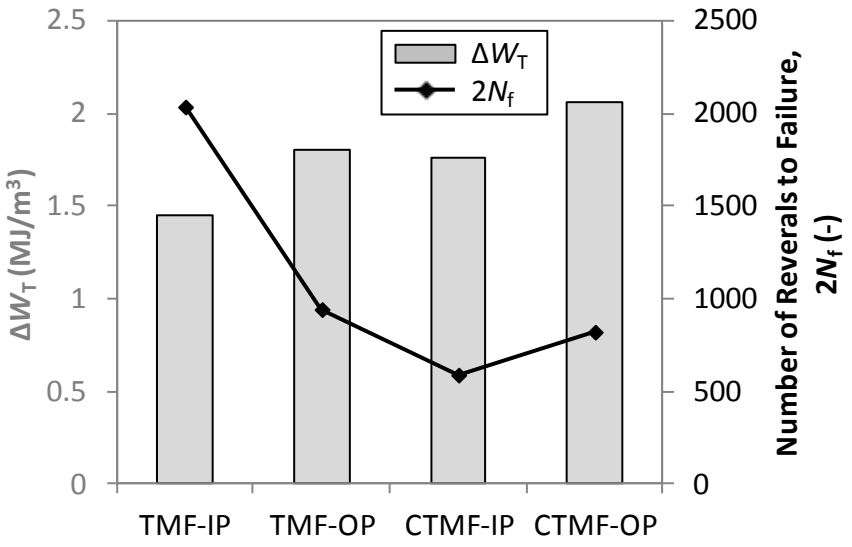

Figure 14: Measured net tensile hysteresis energy and number of reversals to failure compared with test condition in P91 steel at an applied strain-rate of 0.025 %/s and applied strain-range of ±0.5%.

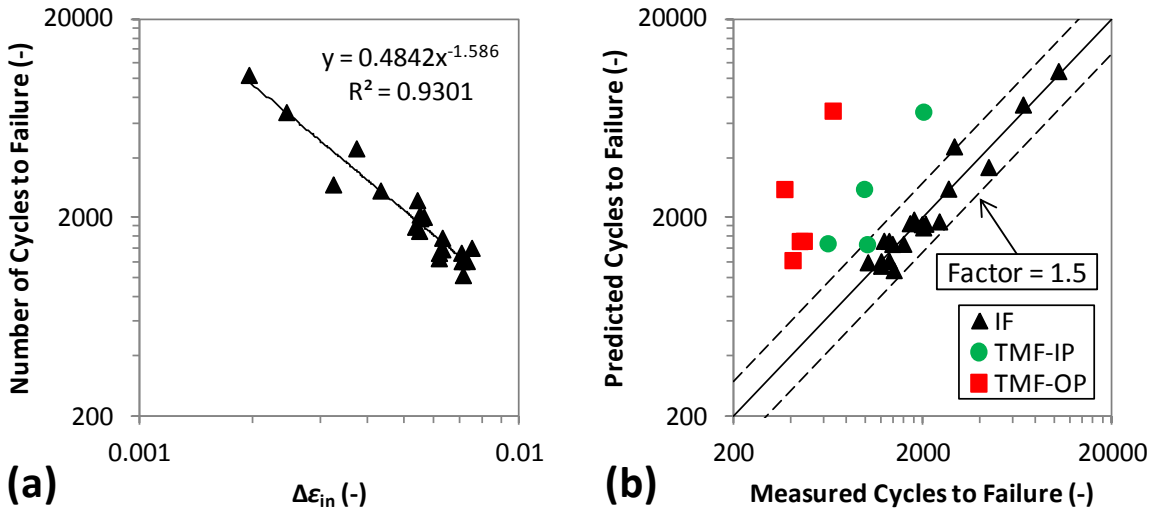

Figure 15: Coffin-Manson (a) parameter identification from IF test data and (b) application to IF and symmetric TMF loading conditions in the 673 K to 873 K temperature range.

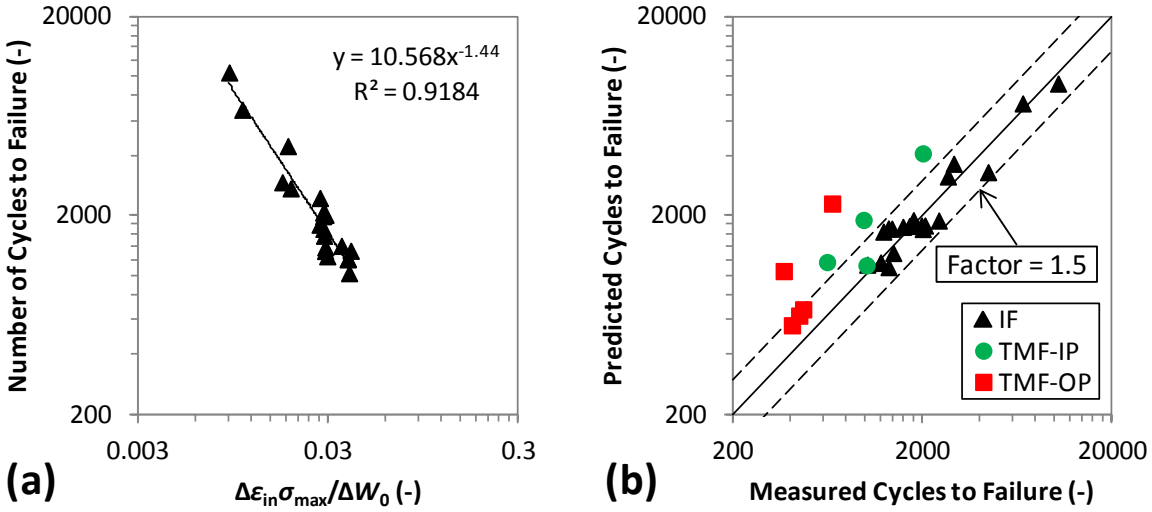

Figure 16: Ostergren model (a) parameter identification from IF test data and (b) application to IF and symmetric TMF loading conditions in the 673 K to 873 K temperature range.

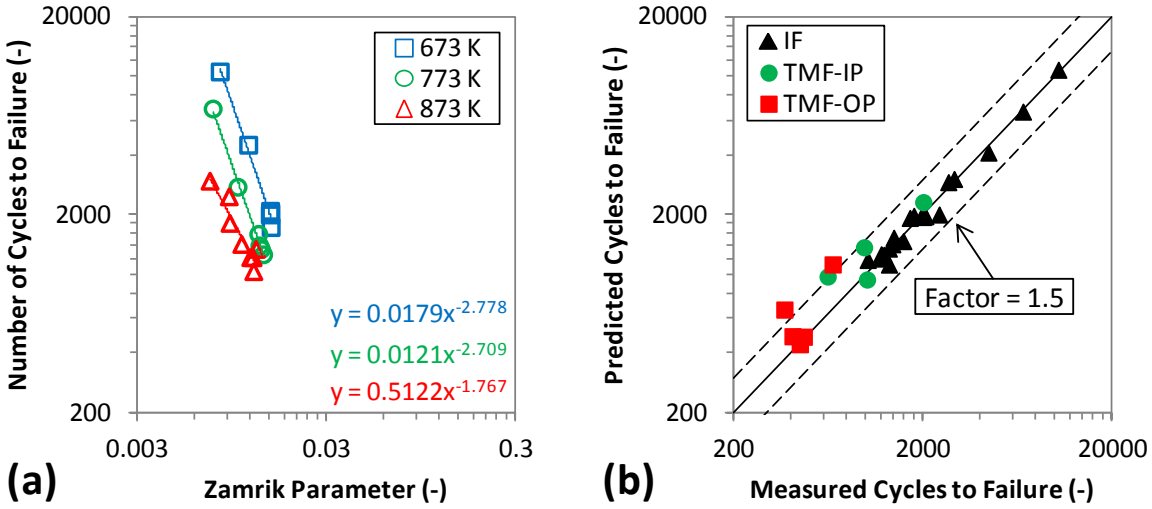

Figure 17: Zamrik model (a) parameter identification from IF test data and (b) application to IF and symmetric TMF loading conditions in the 673 K to 873 K temperature range.

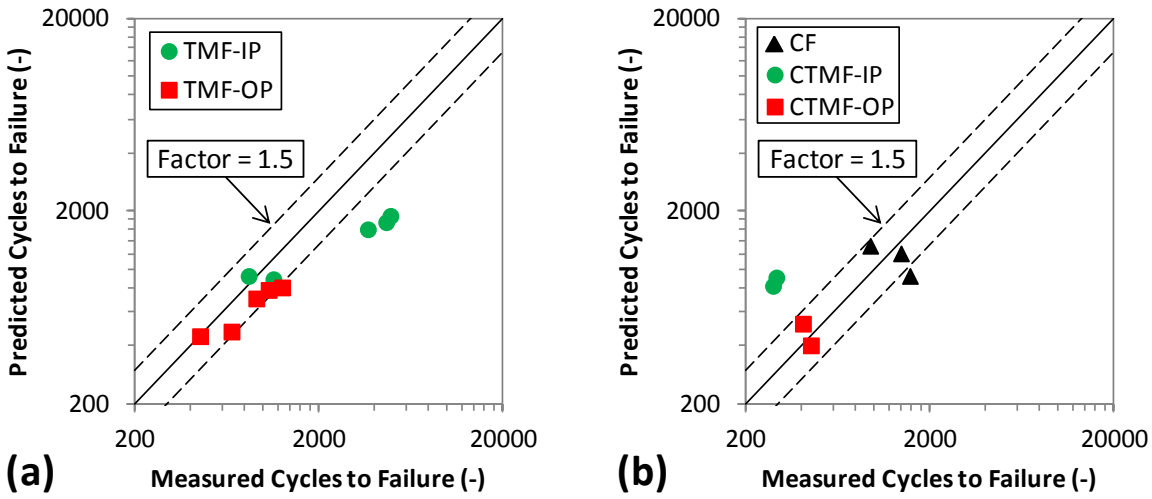

Figure 18: Comparison of measured and Zamrik model predicted fatigue lives for (a) TMF asymmetric tests and (b) IF (673 K, 773 K and 873 K) and TMF with dwell periods.

*Marked Manuscript (will not be used for publication; only for review)

Thermomechanical fatigue in 9-12Cr steels: Life prediction models and the effect of tensile dwell periods

Richard A. Barrett[1,2], Christopher J. Hyde[3], Padraic E. O'Donoghue[2,4], Sean B. Leen[1,2]

[1]*Mechanical Engineering, College of Engineering and Informatics, NUI Galway, Galway, H91 HX31, Ireland*
[2]*Ryan Institute for Environmental, Marine and Energy Research, NUI Galway, Galway, H91 HX31, Ireland*
[3]*Department of Mechanical, Materials and Manufacturing Engineering, University of Nottingham, Nottingham NG7 2RD, UK.*
[4]*Civil Engineering, College of Engineering and Informatics, NUI Galway, Galway, H91 HX31, Ireland*

Corresponding Author: Richard A. Barrett
Email: richard.barrett@nuigalway.ie
Tel.: +353 (0)91 492792

Keywords: 9-12Cr steels; Thermo-mechanical fatigue; Dwell periods; Fatigue life prediction

Abstract: This paper is concerned with the assessment of life prediction models for thermomechanical fatigue (TMF), with specific application to P91 steel. A program of TMF tests, including dwell periods, are performed to determine the role of thermomechanical loading on fatigue life. As expected, fatigue life under conventional TMF testing (no dwells) is governed by maximum applied stress and inelastic strain-range. However, with the introduction of dwell periods, at maximum tensile stress during TMF loading, in-phase loading becomes the life-limiting case. This is attributed here to increased microstructural degradation and oxidation, associated with the dwell at peak temperature. Analysis of commonly used TMF life prediction models shows that the effect of dwell periods currently cannot be predicted for in-phase loading. Thus, it is concluded that physically-motivated approaches are required to successfully predict fatigue life under more complex (service) thermomechanical loading histories.

1. Introduction

The transition to highly flexible operation of power plant to accommodate an ever-increasing share of renewable energy technologies on power grids is leading to an increased frequency of complex start-up and shut-down cycles. This cyclic operation of power plant causes severe thermal gradients, especially on thick-walled components, such as header units. At the same time, higher pressures and temperatures are required for increased efficiency and reduced harmful (e.g. CO_2) emissions. Thus, in conjunction with the increased creep and oxidation deformation induced by the higher temperature operating conditions, critical power plant components are now also being subjected to TMF deformation.

9-12Cr steels are key candidate materials for highly flexible operation of heavy-walled components due to (i) high creep strength, (ii) low-cost relative to other materials and (iii) low coefficient of thermal expansion leading to reduced thermal gradients. The high strength of 9-12Cr steels is achieved by a precipitate and solute strengthened martensitic microstructure. The grain structure consists of prior austenite grains (PAGs), packets, blocks and martensitic laths and subgrains in a hierarchical format, which forms due martensitic

transformation during rapid cooling following austenitisation. The 9-12Cr steels are then tempered to improve toughness and to precipitate $M_{23}C_6$ carbides at grain boundaries (GBs) and MX carbonitrides throughout the microstructure.

To date, a range of high temperature low cycle fatigue (HTLCF) test programs have been completed on 9-12Cr steels across a range of temperatures [1-4]. In all experimental work, a Bauschinger effect is observed due to (i) pinning of dislocations at precipitates [5] and (ii) dislocation pile-ups at GBs within the hierarchical microstructure [6], as well as a significant strain-rate effect, particularly at temperatures in excess of 773 K [4,7]. The primary mechanism of degradation under fatigue in 9-12Cr steels is cyclic softening due to recovery of the low-angle boundary (LAB) dislocation substructure [8]. It is well known that this dislocation substructure is critical for enhanced creep strength, with significant reductions in creep rupture time observed for a coarser initial lath microstructure [9] or prior fatigue loading [10]. Hence, cyclic softening leading to accelerated recovery of the LAB microstructure, as observed in fatigue of 9-12Cr steels, can be expected to have a detrimental effect on highly flexible thermomechanical operation of power plant.

A small number of TMF test programs have been conducted to date on 9-12Cr steels [2,11,12], including both in-phase (TMF-IP) and out-of-phase (TMF-OP) loading conditions. Nagesha *et al.* [2] and Saad *et al.* [12] have investigated the effect of different temperature ranges for both TMF-IP and TMF-OP loading conditions in P91 steel, at constant strain-rates of 1.2×10^{-4} s^{-1} and 1.0×10^{-3} s^{-1}, respectively. It is observed that TMF-IP fatigue life is more sensitive to increasing maximum temperature (T_{max}) when compared to TMF-OP test results. This is attributed to enhanced dynamic recovery and creep deformation as T_{max} increases [2]. However, for TMF-OP loading, where a mean tensile stress exists due to the maximum stress coinciding with T_{min}, fatigue lives are found to be consistently lower than the TMF-IP case [2,11,12]. Along with a mean tensile stress, a significant effect of oxide cracking contributes to premature fatigue failure under TMF-OP conditions. The role of coefficient of thermal expansion mismatch between the matrix material and oxide scale is identified as a primary contributor to oxide-assisted cracking under TMF-OP. The mean tensile stress within the oxide scale is relieved via oxide scale cracking, leading to earlier fatigue crack initiation (FCI) under TMF-OP [13].

In TMF tests conducted in the 573 K to 673 K temperature range in P91 steel at a strain-rate of 1.2×10^{-4} s^{-1} [2], dynamic strain aging (DSA) is found to occur. DSA is detected in P91 steel under isothermal conditions in this temperature range also [14]. In terms of higher TMF temperature ranges, DSA is also observed in a RAFM (9Cr-1W-Mn-V-Ta) alloy at a constant strain-rate of 1.2×10^{-4} s^{-1} in the 673 K to 873 K temperature regime once a threshold (accumulated) plastic strain is exceeded, with no DSA observed under isothermal fatigue (IF) conditions in the same temperature interval [15]. Coupled with oxide cracking and mean tensile stress effects, DSA is found to accelerate FCI and crack growth under TMF-OP conditions. However, no DSA (or serrations) is present in TMF testing of P91 steel under the same temperature interval in the 1.2×10^{-4} s^{-1} to 1.0×10^{-3} s^{-1} strain-rate regime [2,12]. It should

also be noted that the above TMF test programs are completed under constant strain-rate, strain-controlled test conditions with a R_ε-ratio ($R_\varepsilon = \varepsilon_{min}/\varepsilon_{max}$) of -1. No TMF test programs on 9-12Cr steels with a R_ε-ratio other than $R_\varepsilon = -1$ have been published to date.

Previous work by this group has presented a significant strain-rate effect in 9-12Cr steels at temperatures in excess of 773 K [4,7] for IF loading conditions. However, as most laboratory IF and TMF tests are conducted under intermediate to higher strain-rates in the 1.0×10^{-2} s^{-1} to 1.0×10^{-4} s^{-1} range, and above the typical service strain-rates of 1.0×10^{-5} s^{-1} to 1.0×10^{-12} s^{-1} in flexible power plant [3,16], it is necessary to understand the effect of strain-rate under TMF conditions. To date, this key effect has not been investigated for 9-12Cr steels and hence, TMF tests at different strain-rates are presented in this study.

Research to date on TMF of 9-12Cr steels identified the critical interactions of creep, TMF and oxidation as key contributors to failure. Fournier and co-workers [17,18,19] have completed a thorough analysis of the interaction of creep, IF and oxidation in 9-12Cr steels, and Gopinath *et al.* [5] conducted an in-depth study of the effect of dwell time, including damage mechanisms, on fatigue life. In terms of creep-TMF (CTMF) testing in an oxidising environment, very little experimental programs have been undertaken to date. Cui and Wang [20] have completed a creep-TMF test program for a simplified service cycle with dwell periods at maximum, minimum and zero strain, including life prediction using a creep-fatigue (CF) modelling framework. Pan *et al.* [21] used strain energy-based life prediction models [22,23] to predict the effect of phase angle on TMF life for phase angles of 0°, 90° and 180° in a P92 steel without dwell periods. However, to the authors knowledge the effect of phase angle on fatigue life of 9-12Cr steels under thermomechanical loading with dwell periods has not been investigated to date. Thus, this study into the effect of dwell periods at phase angles of 0° and 180° on fatigue life of 9-12Cr steels under TMF, critical loading scenarios for current and next generation highly flexible power plant, represents the first such investigation. The role of R_ε-ratio and strain-rate on TMF response are also examined, with the applicability of empirical TMF life prediction models assessed for conventional and asymmetric TMF, as well as CTMF loading conditions.

2. Methodology

2.1. Material and Heat Treatment

The present study is focused on TMF experimental testing of an ex-service P91 tempered-martensite alloy extracted from a superheater outlet header. In service, this material was subjected to subcritical loading conditions only (T_{max} < 758 K) and was removed from service after 35,168 hrs for purely operational reasons, i.e. there was no evidence of any significant material degradation or damage. Thus, negligible creep deformation and microstructural evolution is assumed prior to the current test program. The chemical composition (in wt.%) is 0.007Al-0.1C-8.48Cr-0.42Mn-0.94Mo-0.058N-0.07Nb-0.19Ni-0.013P-0.26Si-0.204V, with

the balance Fe. The P91 steel was fabricated via a rolling process and underwent a typical two-stage heat treatment process of austenitisation at 1323 K for 0.5 hr, followed by tempering at 1038 K for 1 hr.

2.2. Experimental Testing

The high temperature cyclic behaviour of the P91 steel is measured using the Instron 8862 TMF test rig at the University of Nottingham. The test rig and specimen geometry are described in detail elsewhere [24]. The test program includes IF, CF, TMF and CTMF experiments. All tests were performed under strain-control conditions, with the waveforms illustrated schematically in Figure 1. The complete fatigue test program is summarised in Table 1. IF tests are conducted at temperatures of 293 K to 873 K for three different strain-ranges at higher (0.025 to 0.1 %/s) and intermediate (5×10^{-4} %/s) strain-rates. CF tests, with a 120 s dwell period at maximum (tensile) strain, are conducted at temperatures of 673 K, 773 K and 873 K. The TMF and CTMF experiments consist of both in-phase (IP) and out-of-phase (OP) tests with phase angles of 0° and 180°, respectively. The TMF and CTMF experiments are conducted in the 673 K to 873 K temperature range under several strain-ranges in the higher strain-rate regime. Similar to the IF test program, the CTMF test also has a dwell period at maximum tensile strain, corresponding to a dwell at maximum temperature, T_{max}, for IP conditions and at minimum temperature, T_{min}, for OP conditions. Although a dwell period at T_{max} is a commonly used OP cycle, the proposed OP cycle (with a dwell period at T_{min}) is designed to represent part-load operation of power plant. Dwell periods under such conditions occur at a reduced operating temperature similar in magnitude to the T_{min} value of 673 K tested here. Asymmetric TMF tests, where the maximum tensile strain is significantly higher than the maximum compressive strain, were also performed with R_ε-ratios based on predicted strain in the hoop and axial directions for finite element modelling of a header unit under representative (measured) cyclic operation [3]. Thus, the asymmetric TMF tests were performed under IP and OP conditions, with R_ε-ratios of -0.4 and -0.25, representing the upper and lower bounds of the finite element predicted R_ε-ratios. The maximum applied mechanical strain, from 0.3% to 0.5%, is considered important for thermomechanical loading at discontinuities such as welded connections and T-piece connections [25].

A 20% load drop relative to the load at 150 cycles is set as the criterion for test completion. A typical fatigue crack, as observed during the macroscopic fatigue crack growth (FCG) stage of the test, is presented in the optical micrograph of Figure 2. The number of cycles to failure, N_f, is defined via the ISO 12106:2017-03 standard as a 10% drop in load from the secondary softening stage, as illustrated schematically in Figure 3.

2.3. Fatigue life prediction

At present, a number of prominent models exist for predicting LCF life for both IF and TMF loading conditions. In this section, three such models; namely the (i) Coffin-Manson [26,27], (ii) Ostergren [22] and (iii) Zamrik [23] models are assessed for applicability to P91 steel

under the present TMF loading conditions. According to the Coffin-Manson relationship, the number of cycles to failure, N_f, is defined as:

$$N_f = \frac{1}{2}\left(\frac{\Delta\varepsilon_{in}}{2\varepsilon_f'}\right)^{1/c} \quad (1)$$

where ε_f' is the fatigue ductility coefficient and c is the fatigue ductility exponent. The Ostergren model is defined as:

$$N_f = C(\Delta\varepsilon_{in}\sigma_{max})^{\beta} \quad (2)$$

where C and β are the temperature-dependent Ostergren failure parameters. For the Ostergren model here, the inelastic strain energy ($\Delta\varepsilon_{in}\sigma_{max}$) is normalised with respect to the tensile toughness, ΔW_0, to account for temperature-dependence of the Ostergren model failure constants [30], such that the number of cycles to failure is defined as:

$$N_f = C_1\left(\frac{\Delta\varepsilon_{in}\sigma_{max}}{\Delta W_0}\right)^{\beta_1} \quad (3)$$

where C_1 and β_1 are temperature-independent Ostergren failure constants. Similar to the Ostergren model, the Zamrik model is an energy-based life prediction method, specifically proposed to improve TMF-OP life prediction. It is defined as:

$$N_f = C_2\left(\frac{\varepsilon_{ten}\sigma_{max}}{\varepsilon_f\sigma_{UTS}}\right)^{\beta_2} \quad (4)$$

where ε_{ten} is maximum applied tensile stress, ε_f is material ductility, σ_{UTS} is ultimate tensile strength and C_2 and β_2 are the Zamrik parameters.

3. Results

3.1. Cyclic stress-strain response under IF and TMF

Figure 4 presents the measured stress-strain response for the initial cycle of the P91 steel subjected to TMF-IP and TMF-OP loading in the 673 K to 873 K temperature range at an applied strain-rate of 0.025 %/s. The IF response at temperatures of 673 K and 873 K are also included for comparison. As is evident from Figure 4, the TMF response in both cases is effectively bounded by the IF behaviour for both TMF-IP and TMF-OP loading conditions. Figure 5 shows the cyclic stress-strain response for asymmetric loading under a R_ε-ratio of -0.4 for the initial and 100th cycle under TMF-IP loading, with the TMF-OP response presented in Figure 6 at a R_ε-ratio of -0.25. A minimal strain-rate effect is observed under TMF conditions for the higher strain-rate regime considered here. This is due to minimal time spent at 873 K during TMF testing where a significant strain-rate effect is present in P91 steel, with IF test data at less than 773 K demonstrating a negligible strain-rate effect for the higher strain-rates considered here [7].

The measured stress relaxation during the dwell period of the CTMF tests is presented in Figure 7 for both OP and IP loading conditions. A comparison with isothermal CF

experimental data at the dwell temperatures of 673 K and 873 K, respectively, is also presented. To enable a direct comparison of relaxation behaviour across a range of strain-rates, this data is normalised by the stress at the start of the hold period (σ_0). During this isothermal dwell period in the CTMF cycle at the same applied mechanical strain, the observed relaxation of stress in each case is similar to that of the isothermal CF tests at 673 K for the OP case, as presented in Figure 7a. However, there exists a significant difference in relaxation behaviour for dwells at 873 K (Figure 7b). For the strain-rates considered here, no significant strain-rate effect is observed in P91 steel at temperatures below 773 K [7]. However, a significant strain-rate effect is observed in P91 steel under IF at 873 K, as presented in Figure 8a. Thus, it is concluded here that the observed trend in Figure 7b is primarily due to the strain-rate effect under higher dwell temperatures. Figure 8b demonstrates this strain-rate effect as a function of cycles for CTMF-IP thermomechanical loading conditions in the 673 K to 873 K range, where the dwell occurs at 873 K. Once again, the observed cyclic trend for CTMF is consistent with the strain-rate effect observed under IF conditions at 873 K.

The measured evolution of stress range for the CF (at 673 K and 873 K) and CTMF (IP and OP) tests is presented in Figure 9a. As with all tests conducted within this program, significant cyclic softening is observed in all cases, with only slight differences in the level and rate of softening between CTMF-IP and CTMF-OP loading conditions. Figure 9b presents the accumulated inelastic strain, $p = 2\sum_{i=1}^{N_f} \Delta\varepsilon_{in,i}$, where N_f is the number of cycles to failure and $\Delta\varepsilon_{in,i}$ is inelastic strain range for cycle i, as defined in Figure 10 for CTMF-IP and CTMF-OP loading and comparisons with the corresponding CF data at 673 K and 873 K. The results for CTMF-IP and CTMF-OP suggests a strong dependence of cyclic softening on p, as opposed to temperature, for tests conducted below 873 K. As the primary mechanism of cyclic softening in 9-12Cr steels is LAB dislocation annihilation [8], the hypothesis that cyclic softening is predominantly a function of p is consistent with published observations of negligible LAB evolution under thermal aging conditions [28]. This dependence on p is further realised via the application of Chaboche isotropic stress model to cyclic softening in P91 by Saad *et al.* [12].

3.2. Failure under TMF conditions

Figure 11 presents the effect of symmetric thermomechanical loading (TMF-IP and TMF-OP) on fatigue life as a function of both applied mechanical strain-range and inelastic strain range, $\Delta\varepsilon_{in}$, for P91 steel, including a comparison with IF data. Clearly, thermal cycling leads to a significant reduction in fatigue life, compared with isothermal loading. For symmetric TMF, the most severe case is the TMF-OP case. As the mechanical strain and temperature are out-of-phase, the material is subjected to a significantly higher maximum tensile stress (see Figure 12a) at minimum temperature. This is essentially due to the material reaching a higher maximum stress at the lower temperature (under strain control conditions) and giving a harder response (since maximum tensile stress is a key parameter for FCI). This result

demonstrates the critical role of maximum applied tensile stress, σ_{max}, on fatigue life for symmetric TMF. It should also be noted that there is a significant temperature-dependence for the number of cycles to failure as a function of the applied mechanical strain-range for IF conditions (Figure 11a). However, this temperature-dependence is not as evident when considering inelastic strain-range versus N_f, where the IF test data essentially collapses to a power law relationship as shown in Figure 11b.

Figure 11 also presents a comparison of the observed fatigue life of asymmetric TMF-IP and TMF-OP test results (open symbols). As is evident from this result, the asymmetric TMF tests follow the same trend (qualitatively) as symmetric TMF tests (TMF-OP has reduced fatigue life compared with TMF-IP), albeit under a significantly different relationship with inelastic strain-range for TMF-IP for the strain-ranges considered here. This may represent the transition from low-cycle fatigue to high-cycle fatigue for P91 steel. Thus, further testing at these lower applied strain-ranges under IF and TMF (both symmetric and asymmetric) test conditions is required to define whether this is the transition region for low-cycle fatigue to high-cycle fatigue; this will also provide essential data for plant designers and fatigue life prediction at these potentially crucial strain-ranges for conventional power plant applications.

TMF-OP is similar to isothermal CF (dwell) loading, in which the inelastic strain accumulation is dominant in the compressive part of the loop [13]. The net effect is a mean tensile stress (e.g. see Figure 12b) and hence, reduced fatigue life compared with TMF-IP and IF test data, as illustrated in Figure 11. However, as shown in Figure 13, a significant increase in fatigue life is observed for OP loading with a tensile dwell period (CTMF-OP) when, compared with CTMF-IP test data. This phenomenon is not captured by the mean stress or maximum applied stress effect. This contrasts with the finding for TMF tests without a hold period and highlights (i) the significance of high temperature creep-TMF-oxidation deformation in P91 steels, (ii) the requirement to conduct TMF tests with dwell periods for highly flexible power plant applications and (iii) the requirement to assess current TMF life prediction methodologies for cases of asymmetric TMF and TMF with dwell periods.

3.3. The concept of net tensile hysteresis energy and CTMF behaviour

The net tensile hysteresis energy (ΔW_T) is widely used to evaluate fatigue life [2,29] and is defined schematically in Figure 10 for a CF loading case. Inelastic strain range, $\Delta\varepsilon_{in}$, represents the primary mechanism of energy dissipation at high applied (tensile) stresses, with the dissipated energy predominantly absorbed by the material (the remainder is dissipated as heat to the surroundings). Thus, increasing ΔW_T is nominally consistent with a decreasing fatigue life. Figure 14 presents the measured ΔW_T for TMF-IP and TMF-OP under an applied mechanical strain range of ±0.5% and strain-rate of 0.025 %/s. The ΔW_T is evaluated based on the half-life tensile hysteresis loop area. A significant increase in ΔW_T is observed for the TMF-OP test conditions compared with TMF-IP due to the increased applied stress associated with the reduced temperature during tensile loading. This increase in

ΔW_T is consistent with a decrease in fatigue life. Furthermore, qualitatively, the ΔW_T approach is capable of predicting the observed trend of reduced fatigue life for TMF-OP loading conditions as compared with TMF-IP (e.g. see Figure 14). However, the correlation of N_f with ΔW_T is not valid for CTMF loading conditions. As illustrated in Figure 14, both ΔW_T and fatigue life increase for CTMF loading conditions relative to the corresponding TMF conditions. This is inconsistent with the observed TMF trend that increasing ΔW_T reduces the fatigue life.

3.4. Calibration of fatigue life prediction models for TMF of P91 steel

To apply the Coffin-Manson model to TMF loading in the 673 K to 873 K temperature range, the necessary failure constants (ε_f' and c) are defined using IF data for 673 K, 773 K and 873 K. As is evident in Figure 15a, the data for the three temperatures collapses to approximately a linear relationship for $\Delta\varepsilon_{in}/2$ versus N_f on a log-log plot, with $\Delta\varepsilon_{in}$ taken as the inelastic strain range at half-life. However, as illustrated in Figure 15b, when the same constants are used for TMF loading, the Coffin-Manson relationship predicts extremely non-conservative TMF life compared with experimental data. For the temperature ranges and test conditions considered here, Coffin-Manson is shown to be non-conservative by factors of approximately 6 and 12 for TMF-IP and TMF-OP cases, respectively. This is primarily attributed to the omission of a maximum stress component, an important parameter for TMF life prediction (e.g. see Figure 12a), from the model.

The value of ΔW_0 for P91 steel is identified from monotonic tensile testing of the material [31] and presented in Table 2. The identified failure constants, C_1 and β_1, are 10.57 and -1.44, respectively (see Figure 16a). Figure 16b presents application of the Ostergren model to P91 steel under IF and TMF loading conditions. For TMF loading, $\Delta\varepsilon_{in}\sigma_{max}$, taken at the half-life here, is normalised with respect to ΔW_0 at the maximum cycle temperature (873 K here). As is evident from Figure 16b, extrapolation of the Ostergren model to TMF using failure constants identified from IF data gives non-conservative results, particularly for TMF-OP. If the Ostergren model is normalised with respect to ΔW_0 at the mean temperature (773 K here), the predicted TMF lives are far less conservative. Thus, it is recommended that the Ostergren model be applied with normalisation to ΔW_0 at maximum temperature and that the Ostergren model not be used for TMF-OP loading conditions in 9-12Cr steels.

In Equation (4), $\varepsilon_{ten}\sigma_{max}$ is determined from the half-life hysteresis loop and ε_f and σ_{UTS} are determined from tensile test data as presented in Table 2. Figure 17a presents identification of the temperature-dependent failure constants, C_2 and β_2, from IF data and Figure 17b compares the predicted number of reversals to failure with experimentally observed values for the IF and symmetric TMF cases. The Zamrik model is utilised here with ε_f and σ_{UTS} defined at the maximum temperature, as application at the mean temperature leads to non-conservative results. Although the Zamrik model predicts N_f of symmetric tests quite well (see Figure 17b), this model struggles to predict the fatigue life of (i) asymmetric TMF cycles for the

strain-ranges considered here, as presented in Figure 18a, where results are conservative for the TMF-IP case, and (ii) more importantly, CTMF-IP loading in Figure 18b, where non-conservative results by a factor of approximately 4 are predicted.

4. Discussion

The strain-life failure for symmetric TMF-IP and TMF-OP loading conditions in Figure 11 is consistent with the key roles of maximum tensile stress, σ_{max}, and mean stress, σ_m, in determining fatigue life. Under such loading conditions, ΔW_T can be generally used to correlate fatigue life with life prediction models based on ΔW_T, such as Ostergren (TMF-IP only) and Zamrik. A key benefit of such models is that they can be implemented in multi-axial form in conjunction with critical plane and rainflow cycle counting methods for application to realistic geometries [3,32]. Based on the results of Figure 15 to Figure 17, the Zamrik model performs best for prediction of TMF life, particularly for TMF-OP, whereas the Ostergren model gives significantly non-conservative results. For the Ostergren and Zamrik models, using the maximum temperature as the reference temperature leads to increased conservatism of life prediction. It should also be noted here that the analysis performed does not account for the effect of strain-rate on the mechanical properties and failure constants within the life prediction models; future work should address this effect for strain-rates observed in conventional plant (e.g. 1×10^{-5} s^{-1} to 1×10^{-12} s^{-1}) as $\Delta\varepsilon_{in}$, σ_{max} and σ_{UTS}, for example, depend on strain-rate.

The symmetric TMF test results follow the typical phenomenon of reduced fatigue life for TMF-OP loading compared to TMF-IP (e.g. see Figure 11), with failure driven by a mean tensile stress, as highlighted in Figure 12b. However, the CTMF test program on P91 steel conducted here highlights a contrasting trend, with CTMF-IP loading giving lower fatigue life than the CTMF-OP cases. For CTMF-IP cases considered here, the 120 s dwell period at maximum tensile strain occurs at the maximum temperature of 873 K, where increased microstructural degradation and creep deformation occur. However, for the CTMF-OP case, the dwell period occurs at low temperature, where rate effects and creep deformation are significantly reduced. Furthermore, increased oxidation during a dwell period at higher temperature under CTMF-IP will lead to increased oxide-scale contribution to FCI and hence, reduced fatigue life. Earthman *et al.* [33] have demonstrated this significant effect of oxidation on IF life, and in particular for FCI, in a 12Cr steel. This reduced fatigue life can be attributed to the mechanisms of oxide layer rupture under cyclic mechanical loading [11,13,34], in which rupture of the outermost oxide scale reveals fresh matrix material on which an oxide-scale rapidly forms, with the process repeating until oxide-scale assisted FCI and premature failure occur. As the oxide-scale thickness, h_{ox}, is a function of the temperature-dependent diffusion constant, $D(T)$, i.e. following a parabolic growth law, $h_{ox} = \sqrt{D(T)t}$, the higher dwell temperature of the CTMF-IP test condition will induce increased and accelerated oxide scale growth and, hence, reduced cycles to FCI, as compared with the CTMF-OP case. Thus, for CTMF-IP tests conducted with a dwell period at higher

temperature, the role of oxide scale formation and evolution of the oxide scale on FCI needs to be investigated in more detail for CTMF loading conditions.

As illustrated in Figure 12, the observed TMF-OP and CTMF-OP fatigue lives are quite similar, demonstrating the minimal effect of the 120 s dwell period on fatigue life at 673 K. This is consistent with minimal creep and oxidation damage at temperatures less than 773 K in P91 steels. Thus, it can be concluded that higher temperature dwell periods, e.g. where strain-rate effects and temperature-dependent microstructural degradation become important, can have a detrimental effect on fatigue life. Although conventional power plant components tend to operate with dwell periods on the order of hours, a significant proportion of the thermal stress component relaxes during the initial (rapid) stage of a hold period. For 9-12Cr steels, this initial stage of stress relaxation is on the order of minutes with the stress rapidly decaying to a saturated value [4]. Hence, the 120 s dwell period considered here can qualitatively capture the relaxation behaviour of P91 steel. However, future work will also investigate the effect of dwell time on CF and CTMF performance in 9-12Cr steels to determine the role of microstructural degradation during dwell periods on fatigue life. As the proposed TMF life prediction models follow the trend of reduced fatigue life for increased $\Delta\varepsilon_{in}$ and mean applied stress, these models are not readily applicable to CTMF. Hence, as such dwell periods will become ever more commonplace for current and next generation plant service loading conditions, a fatigue life prediction model which accounts for interactions of creep, TMF and oxidation mechanisms of degradation and FCI is required as the models presented here do not account for microstructural degradation, creep and, potentially most importantly, oxidation effects. For example, Wei *et al.* [35] developed a probabilistic linear superposition crack growth model for creep-fatigue-oxidation during system start-up and shut-down and for 9-12Cr steels, Fournier and co-workers [19] applied a Tanaka-Mura FCI model coupled with crack growth to creep-fatigue-oxidation. Furthermore, the key life limiting factor for 9-12Cr steels under high temperature operation is microstructural degradation, including precipitate coarsening, formation of secondary phase particles (such as Laves phase and Z-phase particles at the expense of solute atoms and carbonitride particles), oxide-scale formation and dynamic recovery. This microstructural degradation, which is dependent on thermal and mechanical loading history, can lead to a significant reduction in strength and the formation of micro-voids [36] and micro-cracks [32], potentially leading to material failure. Thus, microstructure evolution under complex thermomechanical cycles, and its effect on material behaviour, should represent a critical constituent in life prediction and remnant life analysis of power plant components, particularly as higher temperature flexible operation is being pursued. This is even more important in terms of the heterogeneous microstructure of welded connections and their susceptibility to premature failure. Thus, constitutive models should account for the complete array and interdependencies of strengthening mechanisms in 9-12Cr steels [37] and complex microstructural evolution under creep-TMF-oxidation (e.g. significant effect of prior fatigue loading on creep performance of P92 [10]).

5. Conclusions

A program of TMF tests on a P91 steel are presented and current empirical fatigue life prediction models are assessed for applicability to 9-12Cr steels. The key conclusions are:

- In the 673 K to 873 K temperature range considered here, out-of-phase thermomechanical loading is observed to cause a significant reduction in life compared with isothermal fatigue and in-phase thermomechanical fatigue. In such cases, the fatigue life is strongly influenced by the maximum tensile stress.
- When dwell periods are introduced at maximum tensile stress, in-phase loading becomes the critical loading case due to microstructure evolution and accelerated oxide scaling during dwells at peak temperature. This highlights the necessity to complete creep-thermomechanical fatigue testing and the requirement to consider the physical mechanisms of fatigue crack initiation under combined creep, thermomechanical fatigue and oxidation loading conditions.
- Conventional thermomechanical fatigue life prediction models based on inelastic strain energy (e.g. Ostergren and Zamrik) should be used with caution for 9-12Cr steels; such models break down for cases where thermomechanical fatigue loading with high temperature dwell periods.
- Physically-motivated approaches are required to successfully predict fatigue life under complex (service) thermomechanical loading histories. Such approaches must account for microstructural evolution, as well as plasticity- and oxidation-induced mechanisms of fatigue crack initiation.

Acknowledgements

This publication has emanated from research conducted with the financial support of Science Foundation Ireland under Grant Number SFI/14/IA/2604. The authors would also like to acknowledge the contributions made by the collaborators of the MECHANNICS project, including Prof Noel O'Dowd of the University of Limerick.

References

1. Fournier, B., Dalle, F., Sauzay, M., Longour, J., Salvi, M., Caës, C., Tournié, I., Giroux, P.-F., Kim S.-H. Comparison of various 9-12%Cr steels under fatigue and creep-fatigue loadings at high temperature. *Materials Science and Engineering A*, **528** (2011) 6934-6945.
2. Nagesha, A., Kannan, R., Sastry, G.V.S., Sandhya, R., Singh, V., Bhanu Sankara Rao, K. Isothermal and thermomechanical fatigue studies on a modified 9Cr-1Mo ferritic martensitic steel. *Materials Science and Engineering A*, **554** (2012) 95-104.
3. Farragher, T.P., Scully, S., O'Dowd, N.P., Leen, S.B. Development of life assessment procedures for power plant headers operated under flexible loading scenarios. *International Journal of Fatigue*, **49** (2013) 50-61.
4. Barrett, R.A., O'Hara, E.M., O'Donoghue, P.E., Leen, S.B. High temperature low cycle fatigue behaviour of MarBN at 600 °C. *Transactions ASME Journal of Pressure Vessel Technology.*, **138** (2016) 041401.
5. Gopinath, K., Gupta, R.K., Sahu, J.K., Ray, P.K., Ghosh, R.N. Designing P92 grade martensitic steel header pipes against creep-fatigue interaction loading condition: Damage micromechanisms. *Materials and Design*, **86** (2015) 411-420.
6. Chauhan, A., Litvinov, D., de Carlan, Y., Aktaa, J. Study of the deformation and damage mechanisms of a 9Cr-ODS steel: Microstructure evolution and fracture characteristics. *Materials Science and Engineering A*, **658** (2016) 123-134.
7. Barrett, R.A., O'Donoghue, P.E., Leen, S.B. A dislocation-based model for high temperature cyclic viscoplasticity of 9-12Cr steels. *Computational Materials Science*, **92** (2014) 286-297.
8. Sauzay, M., Fournier, B., Mottot, M., Pineau, A., Monnet, I. Cyclic softening of martensitic steels at high temperature - experiments and physically-based modelling. *Materials Science and Engineering A*, **483-484** (2008) 410-414.
9. Ennis, P.J., Zielinska-Lipiec, A., Wachter, O., Czyrska-Filemonowicz, A. Microstructural stability and creep rupture strength of the martensitic steel P92 for advanced power plant. *Acta Materialia*, **45** (1997) 4901-4907.
10. Zhang, W., Wang, X., Gong, J., Jiang, Y., Huang, X. Experimental and simulated characterization of creep behaviour of P92 steel with prior cyclic loading damage. *Journal of Materials Science and Technology*, **33** (2017) 1540-1548.
11. Mannan, S.L., Valsan, M. High-temperature low cycle fatigue, creep-fatigue and thermomechanical fatigue of steels and their welds. *Int. J. Mech. Sciences*, **48** (2006) 160-175.
12. Saad, A.A., Hyde, C.J., Sun, W., Hyde, T.H. Thermal-mechanical fatigue simulation of a P91 steel in a temperature range of 400-600 °C. *Materials at High Temperature*, **28** (2011) 212-218.

13. Nagesha, A., Kannan, R., Sandhya, R., Sastry, G.V.S., Mathew, M.D., Bhanu Sankara Rao, K., Singh, V. Thermomechanical fatigue behaviour of a modified 9Cr-1Mo ferritic-martensitic steel. *Procedia Engineering*, **55** (2013) 199-203.
14. Keller, C., Marguiles, M.M., Hadjem-Hamouche, Z., Guillot, I. Influence of the temperature on the tensile behaviour of a modified 9Cr-1Mo T91 martensitic steel. *Materials Science and Engineering A*, **527** (2010) 6758-6764.
15. Nagesha, A., Kannan, R., Srinivasan, V.S., Parameswaran, P., Sandhya, R., Choudhary, B.K., Mathew, M.D., Jayakumar, T., Rajendra Kumar, E. Thermomechanical fatigue behaviour of a reduced activation ferritic-martensitic steel. *Procedia Engineering*, **86** (2014) 88-94.
16. Nabarro, F. Creep at very low rates. *Metallurgical and Materials Transactions A*, **33** (2002) 213-218.
17. Fournier, B., Sauzay, M., Caës, C., Noblecourt, M., Mottot, M., Bougault, A., Rabeau, V., Pineau, A. Creep-fatigue-oxidation interactions in a 9Cr-1Mo martensitic steel. Part I: Effect of tensile holding period on fatigue lifetime. *International Journal of Fatigue*, **30** (2008) 649-662.
18. Fournier, B., Sauzay, M., Caës, C., Noblecourt, M., Mottot, M., Bougault, A., Rabeau, V., Pineau, A. Creep-fatigue-oxidation interactions in a 9Cr-1Mo martensitic steel. Part II: Effect of compressive holding period on fatigue lifetime. *International Journal of Fatigue*, **30** (2008) 663-676.
19. Fournier, B., Sauzay, M., Caës, C., Noblecourt, M., Mottot, M., Bougault, A., Rabeau, V., Pineau, A. Creep-fatigue-oxidation interactions in a 9Cr-1Mo martensitic steel. Part III: Lifetime prediction. *International Journal of Fatigue*, **30** (2008) 1797-1812.
20. Cui, L., Wang, P. Two lifetime estimation models for steam turbine components under thermomechanical creep-fatigue loading. *International Journal of Fatigue*, **59** (2014) 129-136.
21. Pan, X.-M., Li, X., Chang, L., Zhang, G.-D., Xue, F., Zhao, Y.-F., Zhou, C.-Y. Thermal-mechanical fatigue behaviour and lifetime prediction of P92 steel with different phase angles. *International Journal of Fatigue*, **109** (2018) 126-136.
22. Ostergren, W.J. A damage function and associated failure equations for predicting hold time and frequency effects in elevated temperature, low cycle fatigue. *Journal of Testing and Evaluation*, **4** (1976) 327-339.
23. Zamrik, S.Y., Renauld, M.L. Thermo-mechanical out-of-phase fatigue life of overlay coated IN-738LC gas turbine material. *ASTM Special Publication*, **1371** (2000) 119-137.
24. Hyde, C.J., Sun, W., Leen, S.B. Cyclic thermo-mechanical material modelling and testing of 316 stainless steel. *International Journal Pressure Vessel and Piping*, **87**, (2010) 365-372.
25. Li, M., Barrett, R.A., Scully, S., Harrison, N.M., Leen, S.B., O'Donoghue, P.E. Cyclic plasticity of welded P91 material for simple and complex power plant connections. *International Journal of Fatigue*, **87** (2016) 391-404.

26. Coffin, L.F. A study of the effects of cyclic thermal stresses on a ductile metal. *Transactions of ASME*, **76** (1954) 931-950.
27. Manson, S.S. Behaviour of materials under conditions of thermal stress. *NACA Report 1170*, Lewis Flight Propulsion Laboratory: Cleveland (1953).
28. Panait, C.G., Zielińska-Lipec, A., Koziel, T., Czyrska-Filemonowicz, A., Gourgues-Lorenzon, A.-F., Bendick, W. Evolution of dislocation density, size of subgrains and MX-type precipitates in a P91 steel during creep and during thermal ageing at 600 °C for more than 100,000 h. *Materials Science and Engineering A*, **527** (2010) 4062-4069.
29. Song, G., Hyun, J., Ha, J. Creep-fatigue life prediction of aged 13CrMo44 steel using the tensile plastic strain energy. In: Rémy, L., Petit, J. (Eds.) Temperature-Fatigue Interaction. Elsevier Applied Science: London (2002) 65-73.
30. Lee, K.-O, Hong, S.-G., Lee, S.-B. A new energy-based fatigue damage parameter in life prediction of high temperature structural materials. *Materials Science and Engineering A*, **496** (2008) 471-477.
31. Golden, B.J., Li, D.-F., Tiernan, P., Scully, S., O'Dowd, N.P. Deformation characteristics of a high chromium power plant steel at elevated temperatures. *Proceedings of the ASME 2015 Pressure Vessel and Piping Conference (PVP2015)*, Boston, Massachusetts, USA, July 19th - 23rd, 2015.
32. O'Hara, E.M., Harrison, N.M., Polomski, B.K., Barrett, R.A., Leen, S.B. The effect of inclusions on the high-temperature low-cycle fatigue performance of cast MarBN: Experimental characterisation and computational modelling. *Fatigue and Fracture of Engineering Materials and Structures*, **41** (2018) 2288-2304.
33. Earthman, J.C., Eggeler, G., Ilschner, B. Deformation and damage processes in a 12%Cr-Mo-V steel under high temperature low cycle fatigue conditions in air and vacuum. *Materials Science and Engineering A*, **110** (1989) 103-114.
34. Neu, R.W., Sehitoglu, H. Thermomechanical fatigue, oxidation and creep: Part I. Damage mechanisms. *Metallurgical Transactions A*, **20** (1989) 1755-1767.
35. Wei, Z., Yang, F., Lin, B., Luo, L., Konson, D., Nikbin, K. Deterministic and probabilistic creep-fatigue-oxidation crack growth modelling. *Probabilistic Engineering Mechanics*, **33** (2013) 126-134.
36. Pandey, C., Saini, N., Mahapatra, M.M., Kumar, P. Study of the fracture surface morphology of impact and tensile tested cast and forged (C&F) Grade 91 steel at room temperature for different heat treatment regimes. *Engineering Failure Analysis*, **71** (2017) 131-147.
37. Barrett, R.A., O'Donoghue, P.E., Leen, S.B. A physically-based high temperature yield strength model for 9Cr steels. *Materials Science and Engineering A*, **730** (2018) 410-424.

Tables

Table 1: High temperature cyclic test program on P91 steel.

Test Type	***Temperature* (K)**	***Strain range* (%)**	***Strain-rate* (%/s)**	***Waveform***
IF	293, 673, 773 and 873	±0.5 ±0.5 ±0.4 ±0.3 ±0.5	0.1 0.033 0.033 0.033 0.025	R_ε = -1 (Triangular)
IF	673, 773, 823, 873 and 898	±0.3	5×10^{-4}	R_ε = -1 (Triangular)
CF	673, 773 and 873	±0.3	0.1	120 s hold period (Triangular)
TMF (IP & OP)	673 to 873	±0.5 ±0.5 ±0.5 ±0.4 ±0.3	0.033 0.025 0.01 0.033 0.033	R_ε = -1 (Triangular)
TMF (IP & OP)	673 to 873	+0.5,-0.2 +0.5,-0.2 +0.4,-0.1 +0.4,-0.1 +0.4,-0.1	0.033 0.025 0.033 0.025 0.01	R_ε = -0.4; R_ε = -0.25 Asymmetric (Triangular)
CTMF (IP & OP)	673 to 873	±0.5	0.033 0.025	120 s hold period (Triangular)

Table 2: Measured monotonic properties of P91 steel for Ostergren and Zamrik models.

***T* (K)**	**ΔW_0 (MJ/m^3)**	**σ_{UTS} (MPa)**	**ε_f (%)**
293	109	690.2	17.9
673	78	612.0	25
773	71	530.0	16.2
873	43	391.4	18.7

Figures

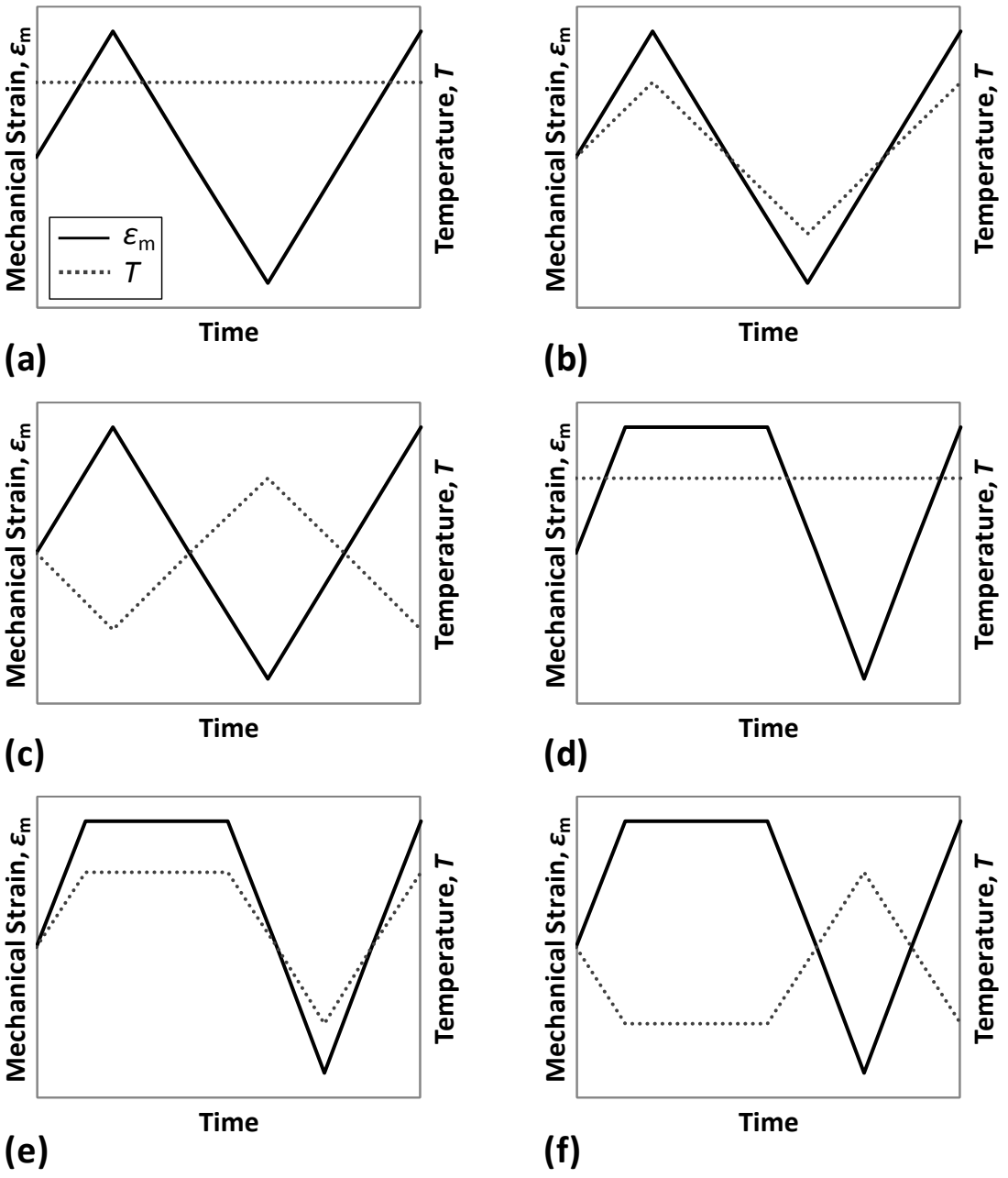

Figure 1: IF, TMF and CTMF waveforms in the test program: (a) IF, (b) TMF-IP, (c) TMF-OP, (d) CF, (e) CTMF-IP and (f) CTMF-OP.

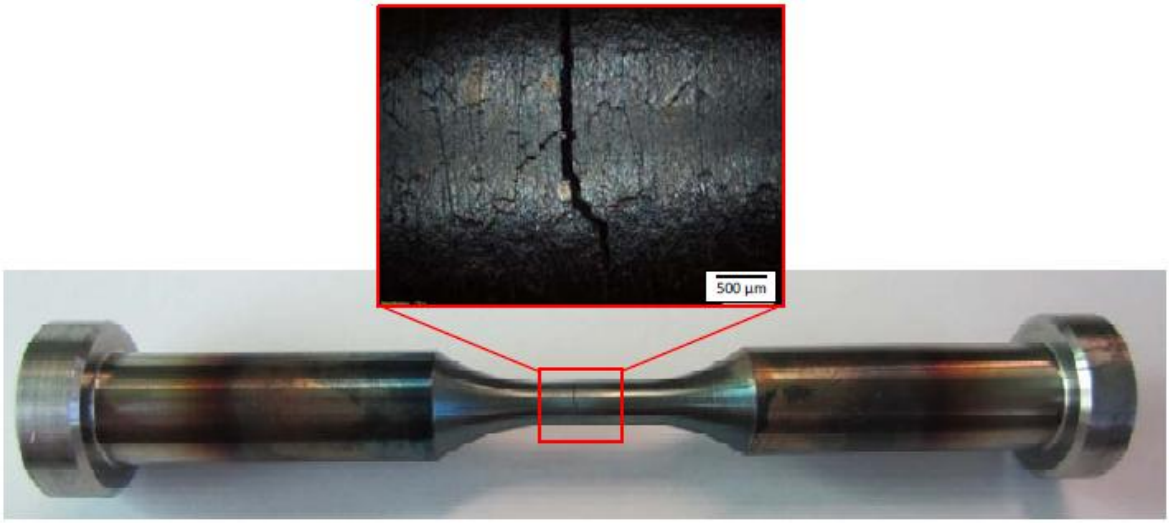

Figure 2: TMF specimen post-test and optical micrograph of the dominant fatigue crack under a failure criterion of a 20% drop in load after 150 cycles (inset).

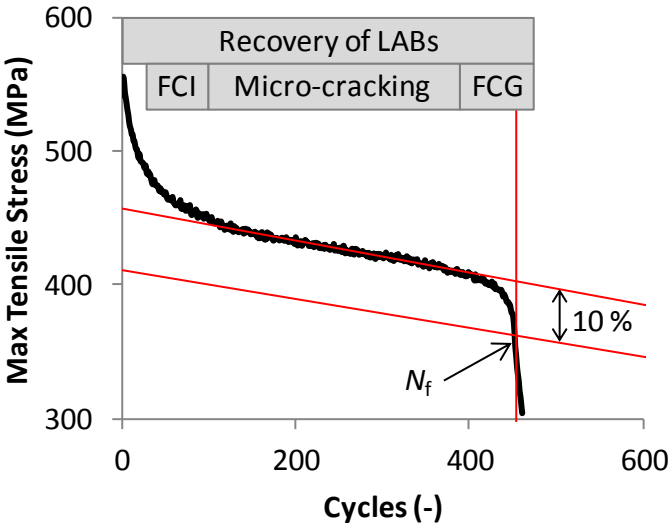

Figure 3: Cyclic softening of P91 steel under TMF-IP loading with deformation mechanism map highlighting recovery (lath widening and particle coarsening), fatigue crack initiation (FCI), coalescence to form micro-cracks and macroscopic fatigue crack growth (FCG).

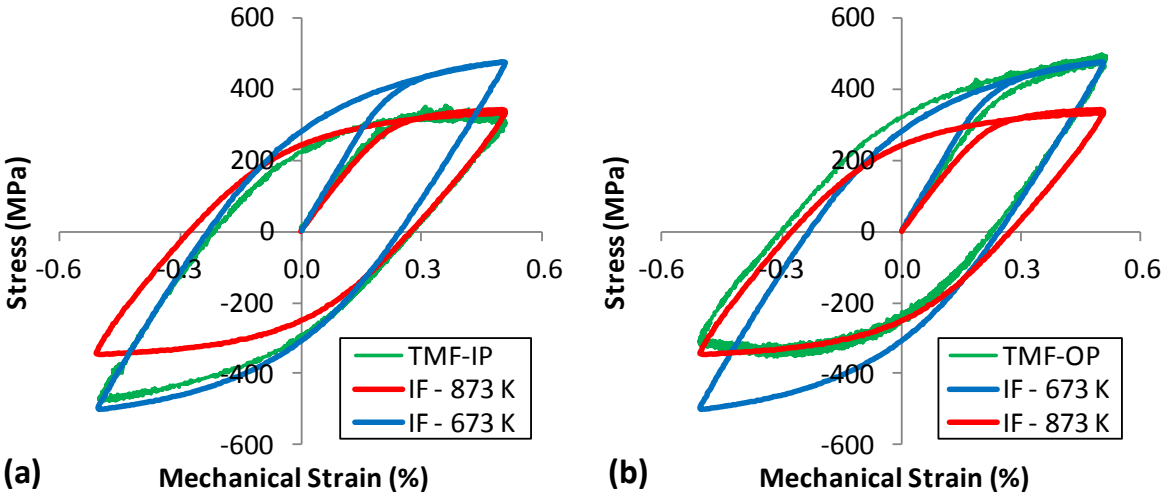

Figure 4: Comparison of (a) TMF-IP and (b) TMF-OP cyclic stress-strain response with IF data at 673 K and 873 K for the initial cycle at an applied strain-rate of 0.025 %/s and mechanical strain-range of ±0.5%.

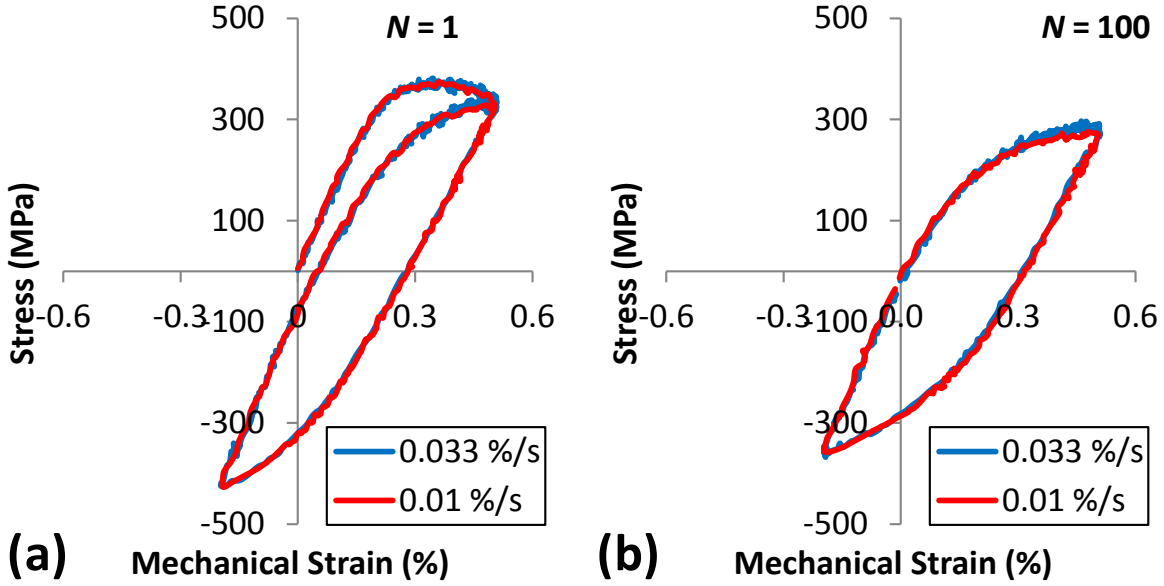

Figure 5: TMF-IP behaviour of P91 steel under asymmetric TMF testing for the (a) initial and (b) 100th cycle in the 673 K to 873 K temperature range under a R_ε-ratio of -0.4.

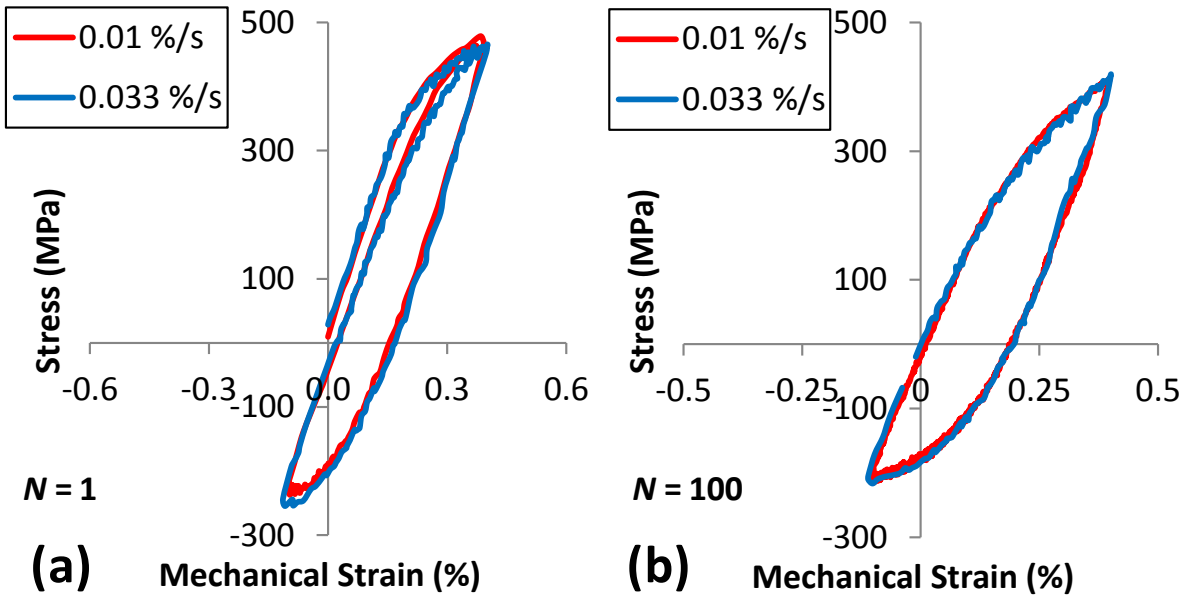

Figure 6: TMF-OP behaviour of P91 steel under asymmetric TMF testing for the (a) initial and (b) 100th cycle in the 673 K to 873 K temperature range under a R_ε-ratio of -0.25.

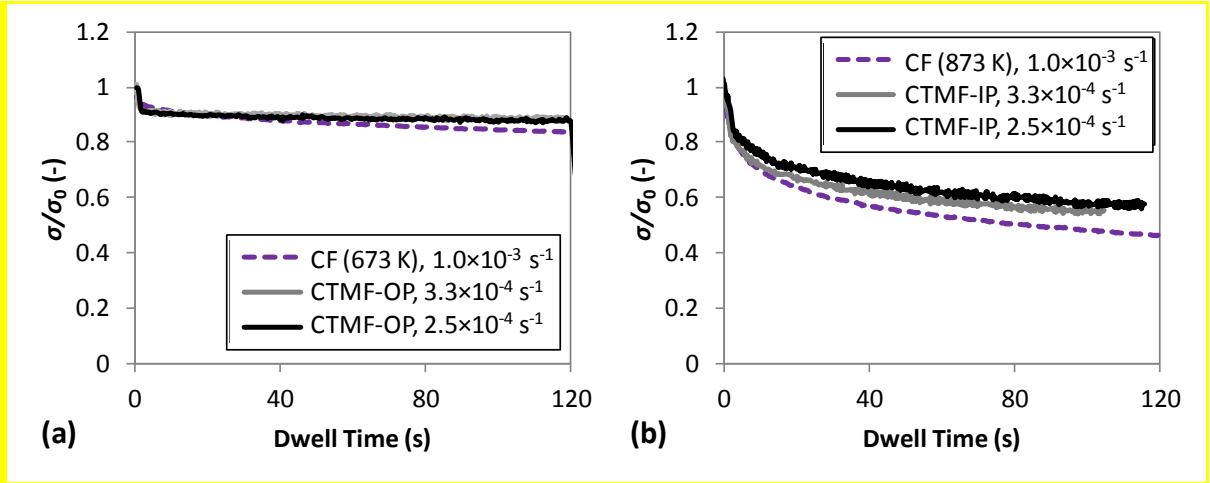

Figure 7 Comparison of the measured (a) CTMF-OP and (b) CTMF-IP stress response during the dwell period (solid lines) for two different strain-rates of 3.3×10^{-4} s^{-1} and 2.5×10^{-4} s^{-1}. A comparison with isothermal CF experimental data at the dwell temperature is also included (dotted lines) at an alternate strain-rate of 1.0×10^{-3} s^{-1}. The stress values are normalised with respect to the initial stress at the start of the hold period. The applied mechanical strain during the dwell period is 0.5% in all cases.

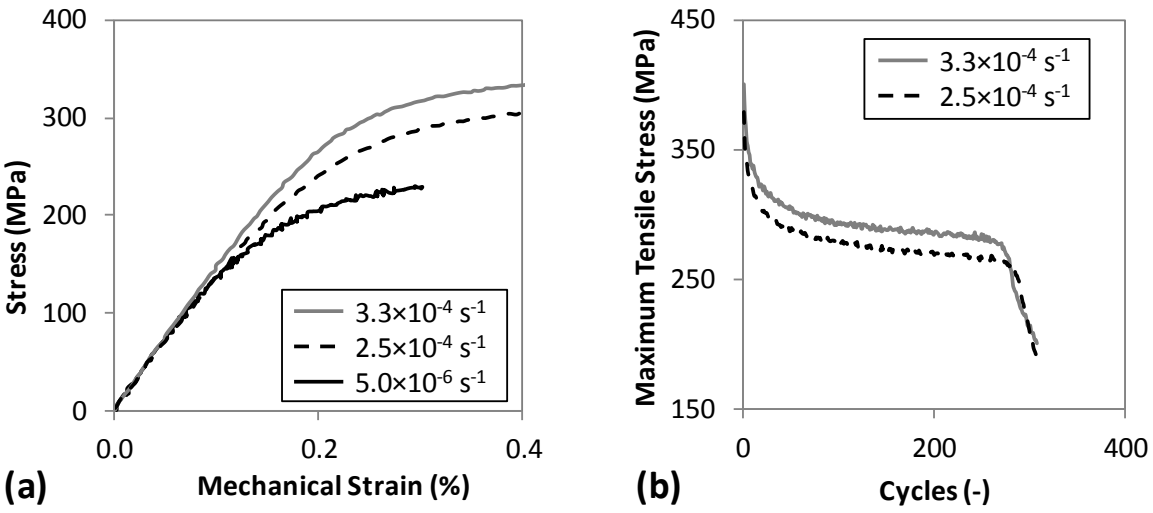

Figure 8: Effect of strain-rate on (a) tensile stress-strain response under IF loading at 873 K and (b) evolution of maximum tensile stress with increasing cycles under CTMF-IP loading.

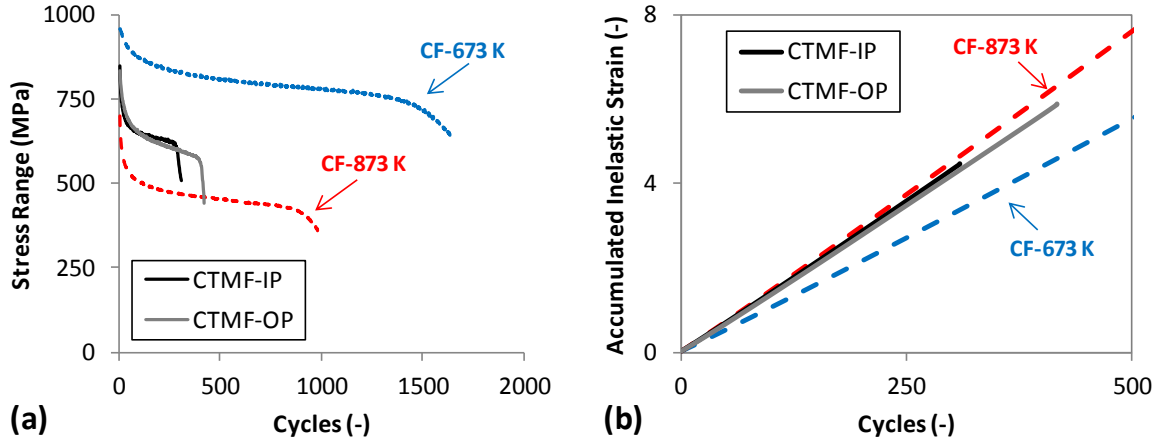

Figure 9: Measured cyclic evolution of (a) stress range and (b) accumulated effective inelastic strain for CF (dashed lines) and CTMF (IP and OP, solid lines) test conditions in the 673 K to 873 K temperature range.

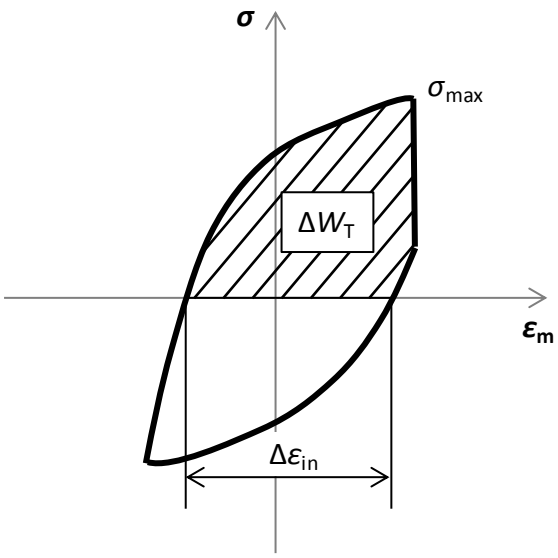

Figure 10: Schematic representation of the net tensile hysteresis energy in a CF test.

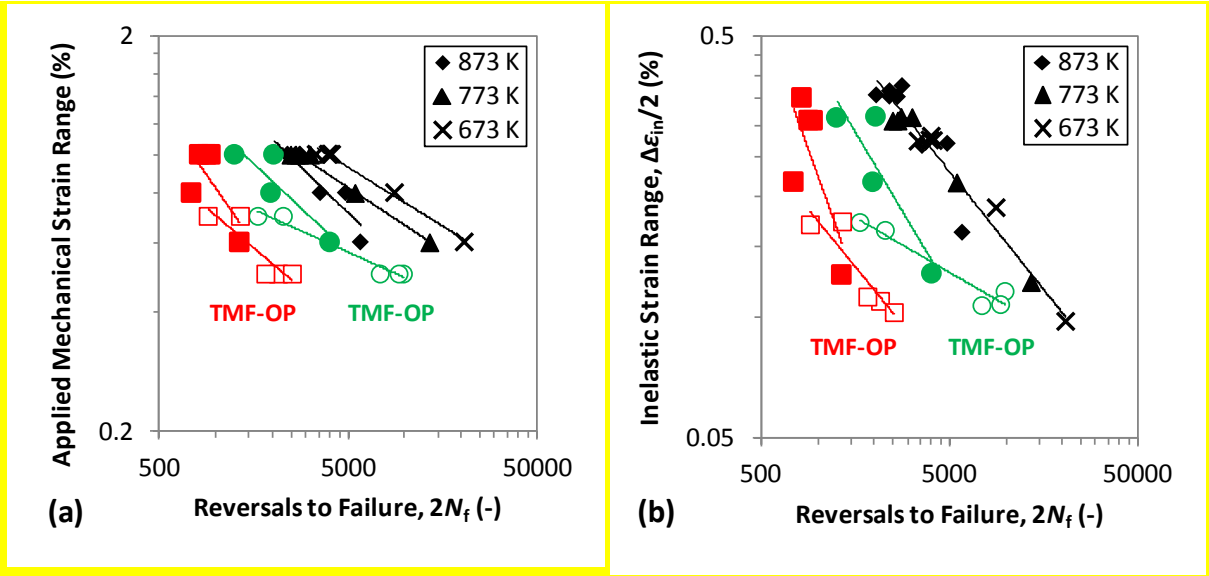

Figure 11: Number of reversals to failure as a function of (a) total applied strain-range and (b) inelastic strain-range for IF (673 K, 773 K and 873 K) and TMF-IP and TMF-OP in the 673 K to 873 K temperature range. Symmetric TMF results are in full symbols and asymmetric TMF test results are in open symbols.

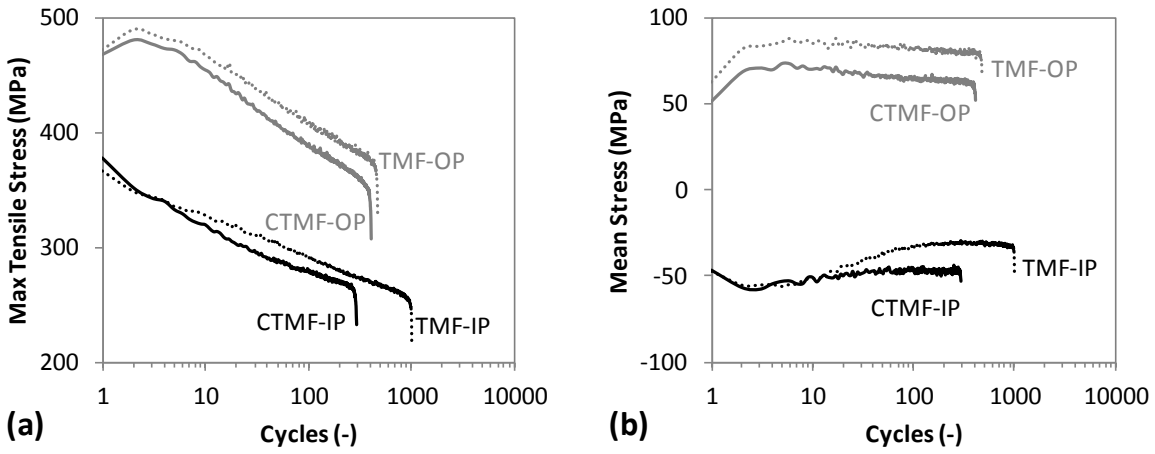

Figure 12: Cyclic evolution of (a) maximum tensile stress and (b) mean stress for TMF and CTMF loading under IP and OP thermo-mechanical conditions. The strain-rate is 0.025 %/s and applied mechanical strain is ±0.5%.

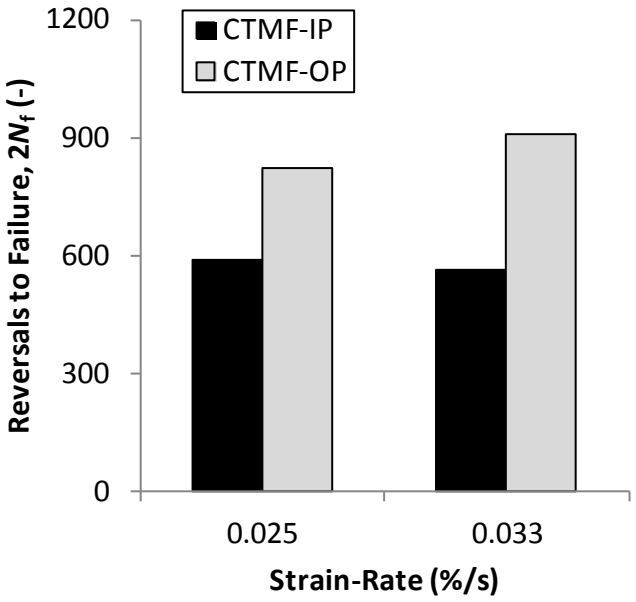

Figure 13: Increased reversals to failure associated with CTMF-OP loading condition compared with CTMF-IP behaviour for an applied mechanical strain is ±0.5% at two different strain-rates.

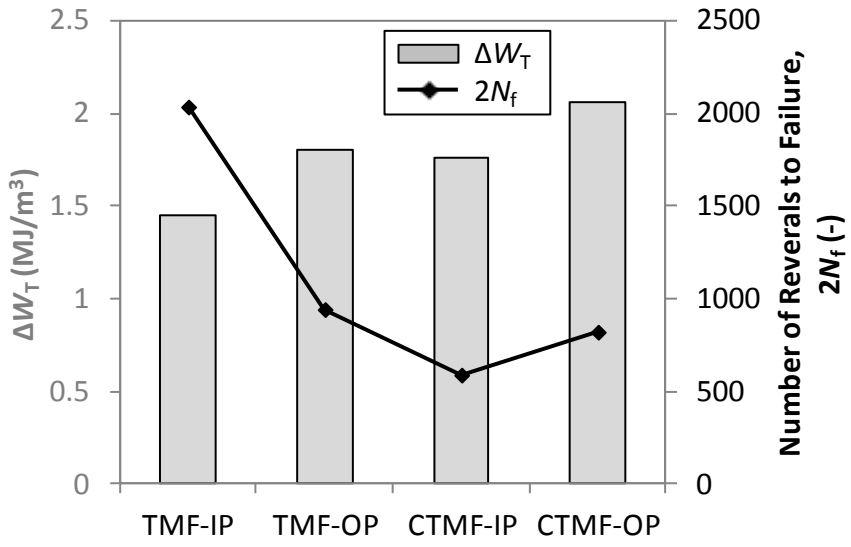

Figure 14: Measured net tensile hysteresis energy and number of reversals to failure compared with test condition in P91 steel at an applied strain-rate of 0.025 %/s and applied strain-range of ±0.5%.

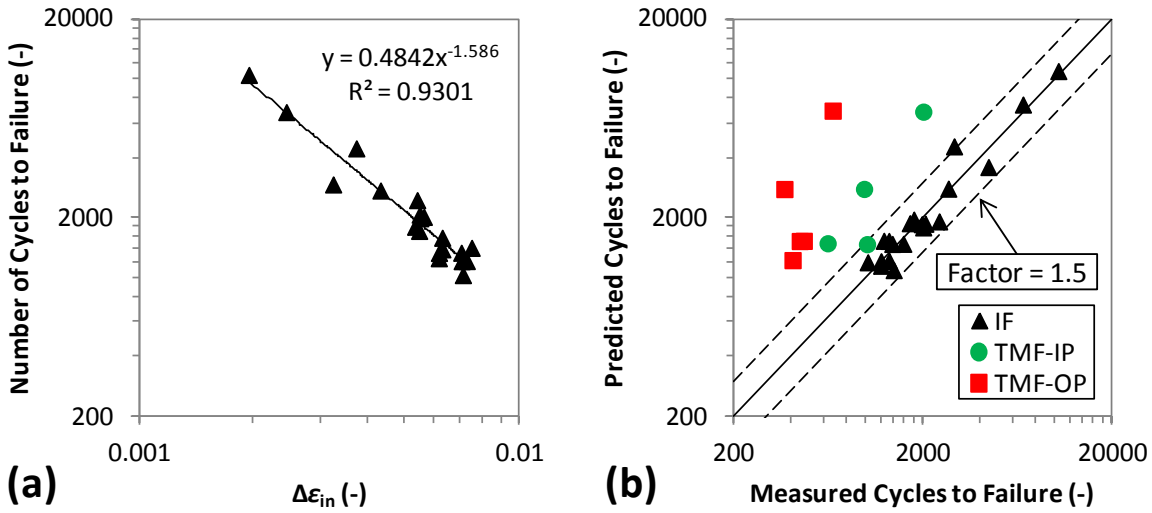

Figure 15: Coffin-Manson (a) parameter identification from IF test data and (b) application to IF and symmetric TMF loading conditions in the 673 K to 873 K temperature range.

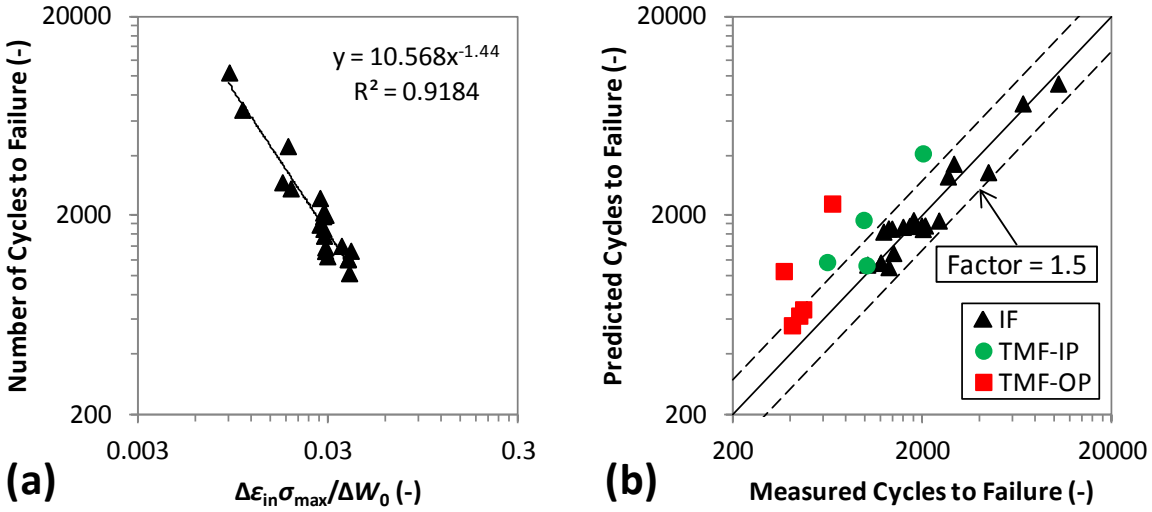

Figure 16: Ostergren model (a) parameter identification from IF test data and (b) application to IF and symmetric TMF loading conditions in the 673 K to 873 K temperature range.

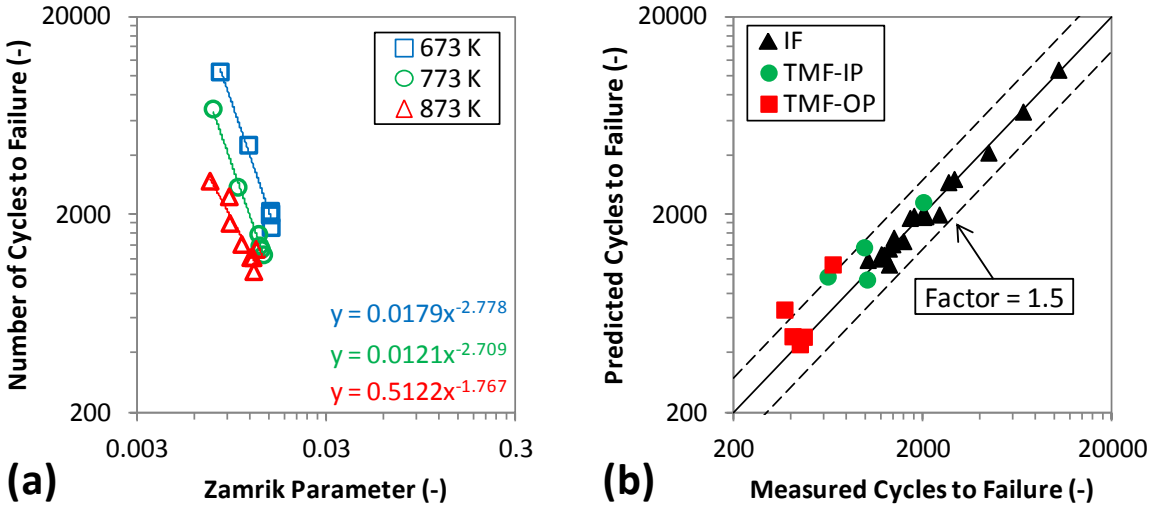

Figure 17: Zamrik model (a) parameter identification from IF test data and (b) application to IF and symmetric TMF loading conditions in the 673 K to 873 K temperature range.

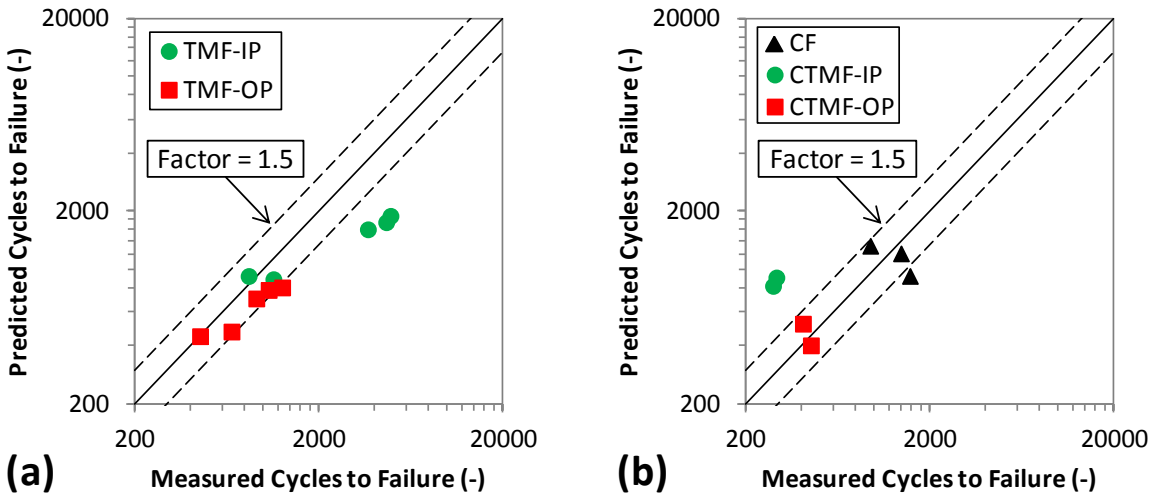

Figure 18: Comparison of measured and Zamrik model predicted fatigue lives for (a) TMF asymmetric tests and (b) IF (673 K, 773 K and 873 K) and TMF with dwell periods.